Verification of a 3D External Photon Beam Treatment Planning System

by

Anas Orfali
Medical Physics Unit
McGill University, Montreal
August, 1996

A thesis submitted to the Faculty of Graduate Studies and Research
in partial fulfillment of the requirements for the degree of
Master of Science in Medical Radiation Physics

ISBN 0-612-19840-5

Canada

Abstract

Treatment planning is recognized as a fundamental step in clinical radiotherapy. The increased availability and complexity of three dimensional (3D) computerized treatment planning systems necessitates a full verification protocol to be completed prior to the implementation of the treatment planning system in routine use.

We have designed and performed a detailed experimental verification program aimed at evaluating each individual dosimetric aspect of our 3D computerized treatment planning system (Varian CADPLAN, version 2.62). The verification tests ranged in complexity from the most basic standard geometry to a simulation of a full treatment case. Results from each individual testing geometry are presented, and an overall evaluation is discussed. We have concluded that our 3D treatment planning system is acceptable for clinical use.

Résumé

Une étape fondamentale d'une cure de radiothérapie consiste en une simulation par ordinateur de la distribution de dose que recevra le patient lors de son traitement. Aujourd'hui, la grande complexité des systèmes de simulation par ordinateur exige une vérification exhaustive de la performance avant la mise en service clinique du système de simulation.

Nous avons élaboré, et ensuite appliqué, une gamme de tests permettant d'évaluer séparément les diverses caractéristiques dosimétriques du système de simulation à trois dimensions (3D) installé à notre hôpital (Varian CADPLAN version 2.62). Dans ce mémoire, nous présentons les résultats de notre gamme de tests, nous comparons des simulations simples et complexes à des mesures, et nous terminons avec une discussion générale de la performance du système de simulation 3D, que nous constatons adéquat pour le service clinique.

Acknowledgments

I would like to express my endless gratitude to my supervisor, Dr. Ervin B. Podgorsak, for placing his trust in me and giving me the freedom to work independently while at the same time maintaining his open door policy of guidance to all students in general and to me in particular. Dr. Podgorsak was an exemplary supervisor who, in spite of his busy schedule, would always have time for students. This thesis was produced at the Medical Physics Unit of the Montreal General Hospital. The financial support for the duration of this degree was provided mainly by Fonds pour la Formation de Chercheurs et l'Aide à la Recherche (FCAR) and also partly by the support of the Medical Research Council through Dr. Podgorsak. I am very thankful for the support of FCAR, without which this might not have been possible.

I am also thankful to the clinical physics staff and to the engineers at the Medical Physics Unit, especially Marina Olivares for introducing me to the world of TLDs and Joe Larkin for all the resuscitation efforts that he tried on my computer. I would like to recognize the endless contributions of my fellow colleague and office-mate, Arthur Curtin-Savard, for putting up with me for so long and for all the interesting discussions and the extremely helpful attitude he showed at all times. He was also very kind in sharing his computing facilities in times of need and provided much needed help in the French translation of the abstract.

I am, however, mostly in debt to my parents, Mrs. Najah Traboulsi and Dr. Fayez A. Orfali, who are the main reason for any success that I might reach. I fully and completely attribute all my achievements and accomplishments to them. I am also in debt to my older brother and sister who gave me the ideal environment in which to thrive throughout the years.

This thesis is dedicated to my parents.

Preface

This thesis is aimed at designing and applying an experimental verification program of a three dimensional external photon beam treatment planning system. The experimental methods are first evaluated and their uncertainties are determined. Then a thorough dosimetric verification of the treatment planning system is carried out covering a wide range of planning aspects from standard geometries, through inhomogeneity correction, to a simulation of a clinical case.

Chapter 1 provides an overall description of the radiation therapy process and the importance of treatment planning in this process. The motivation for the thesis is also discussed.

Chapter 2 describes the basic concepts and terminology required for the understanding of succeeding discussions in the thesis.

Chapter 3 outlines the rationale in the design of verification tests and their acceptability criteria. A thorough discussion of 3D treatment planning systems in general and our system in particular is also presented.

Chapter 4 considers the dosimetry methods used and evaluates their reproducibility and the effect of various factors on their response.

Chapter 5 presents the results of standard and complex test geometries and addresses the shortcomings of the treatment planning system at each particular case.

Chapter 6 is devoted to the verification of the inhomogeneity correction algorithms available in our treatment planning system. The results of the tests are presented and a simulated clinical cases is also evaluated.

Chapter 7 summarizes the overall results and addresses the dosimetric and non-dosimetric performance of the treatment planning system.

Table of Contents

Chapter 3:
Treatment Planning Systems

Chapter 4:
Dosimetry Techniques

Chapter 5:
Verification of the Three Dimensional Computerized Dose Calculation

Chapter 6:
Inhomogeneity Correction

Chapter 7:
Performance Evaluation and Quality Assurance of the Treatment Planning System

Chapter 1:
Overview of the Radiation Treatment Process

1.1 Introduction

Radiation therapy is a branch of medicine defined by the application of radiation, in various forms and from various sources, for the purpose of treatment of disease. Radiation beams have been primarily used for tumor treatment, both malignant and non-malignant; however, radiation also finds clinical application in some other areas, such as in treatment of anatomic malformations, e.g., arteriovenous malformations or in treatment of functional disorders. Along with chemotherapy and surgical procedures, radiation therapy is a well established method for tumor tissue control. Radiation treatment can be applied from an external source (*external beam radiotherapy*) or an internal source (*brachytherapy*). The project described in this thesis was focused on external photon beams produced by a number of machines that differ in their design and operation, e.g., betatrons, linear accelerators, isotope machines, etc.

The most widely used sources for external beam radiotherpy are the *linear accelerator* and the *cobalt-60* unit. Linear accelerators (linacs) produce photons mainly through the *bremsstrahlung* process which is accomplished by accelerating a beam of electrons up to a certain kinetic energy and then directing the electrons onto a target. The electrons are decelerated within the target material and photons are produced according to the Larmor relationship. Cobalt units, on the other hand, reiy on an intrinsic nuclear reaction of the

cobalt-60 isotope which through a beta minus decay into nickel-60 leads to the production of gamma rays with two photon energies: 1.17 MeV and 1.33 MeV.

For external photon beam radiotherapy, the Montreal General Hospital is equipped with one cobalt-60 unit (AECL Theratron-780) and three linear accelerators: SHM Therapi-4 (4 MV), Varian Clinac-18 (10 MV) and Varian Clinac-2300 C/D (6 MV and 18 MV). The work in this thesis was exclusively concentrated on the cobalt-60 beam from the T-780 unit and the 10 MV photon beam from the Clinac-18 linac.

1.2 The radiotherapeutic process

The steps involved in radiotherapy are numerous and rely on the cross-collaboration of knowledge from various fields to ensure optimal patient care. The diagram in Fig. 1.1 illustrates the typical progress of a patient through the radiotherapy department starting with the initial entry to the clinic/hospital, through the administration of fractionated treatment, to regular follow-up visits on a monthly and yearly basis after completion of treatment. The outlined scheme is a typical process which may differ in detail from one center to the other.

The first step in tumor care is the *diagnosis*, which is performed by various specialists depending on the tumor location. The diagnostic step may include a physical examination of the tumor site, palpation, direct extraction of tissue samples (biopsy), or the acquisition of Computed Tomography (CT), Magnetic Resonance (MR) or Ultrasound (US) images. Typically, radiation therapy is combined with other treatment modalities, e.g., surgery or chemotherapy, in order to ensure a high *tumor control probability (TCP)* and to reduce the morbidity and risk of recurrence after the treatment.

After the use of external radiation therapy is agreed upon, the patient is taken for treatment *simulation* in the radiotherapy department. This is done under the direction of a radiation oncologist using the "simulator" machine, which contains a diagnostic x-ray tube mounted on a head that emulates the

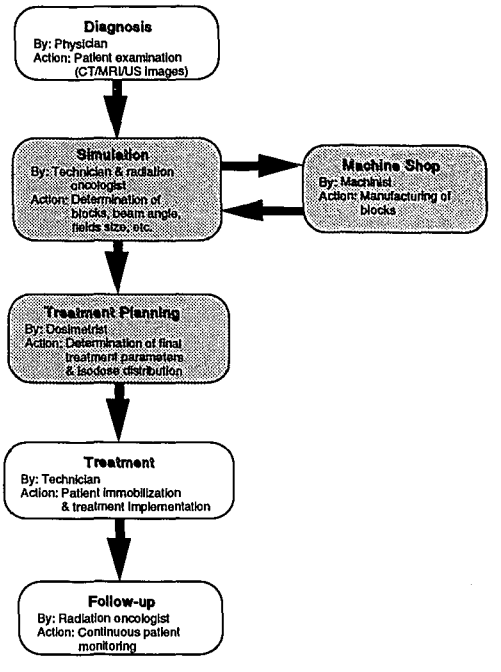

FIG. 1.1. *A simplified, typical scheme of the various steps in radiation therapy. Shaded boxes represent stages where medical physics may be directly or at least indirectly involved (CT: computed tomography; MRI: magnetic resonance imaging; US: ultrasound).*

mechanical behavior of an external beam treatment unit be it a cobalt unit or a linac. During the simulation, the position of critical organs, the position of the beam isocenter (for isocentric treatments), the use of beam blocks, and the shape of the patient's contour are determined. These tasks are greatly facilitated, with the presence of a fluoroscopy option on the simulator. The entry positions of the proposed treatment beams are also determined and marked on the patient's skin. The simulation procedure is often done in the presence of the radiation oncologist and the technician. The machinist may be called upon if blocks or certain beam modifiers are needed, in which case he/she is given the

exact shape and dimensions of the required shielding piece. Treatment simulation can also be accomplished *virtually* by using the CT-simulator, which is an ordinary CT scanner equipped with positioning laser beams that enable an accurate external localization of the collected CT images. These CT images are then manipulated by ray tracing software which simulates the treatment digitally. The *clinical target volume* is then determined by the radiation oncologist, using either the CT/MR images, or during the CT-simulation by delineating the outline on the digitally reconstructed radiographic (DRR) film.

Using the patient data collected from the simulation process and the diagnosis stage, the dosimetrist then determines the appropriate treatment parameters by generating a *treatment plan* (a clinical physicists may be involved during this stage for difficult cases). The final treatment plan is verified by a clinical physicist and has to be approved by the radiation oncologist who prescribes a certain target dose to a specific isodose surface based on his/her experience, type of disease, and location of the target and neighboring sensitive structures. Instead of delivering the entire prescription dose in one treatment session, the treatment is usually divided into relatively small fractions, with the purpose of achieving tumor control and reducing the harmful effects of radiation on healthy tissue. The fractionation scheme is also determined by the radiation oncologist.

At this stage, the patient has finally reached the *treatment step*, where the treatment technician (currently referred to as radiation therapist in the United States) calculates the appropriate treatment time (for the cobalt-60 unit) or monitor unit setting (for the linac). The patient is then positioned on the treatment table and immobilized using appropriate immobilization devices. The treatment is carried out by the technician. During the treatment, a film is exposed, and kept with the patient's record. This film, which is often given the term *portal film or check film*, is used for the verification of the proper patient positioning (done by comparing the portal film with the simulation film obtained earlier), and it also serves as a permanent legal record of the treatment delivered. New linacs incorporate electronic portal imaging devices (EPID) for this purpose.

1.3 Overview of treatment planning

The purpose of radiation treatment is the elimination of cancerous cells constituting a tumor while sparing the normal tissues any harm or damage. In other words, optimal radiation treatment aims at maximizing the *tumor control probability* (TCP) while simultaneously having the *normal tissue complication probability* (NTCP) at the absolute minimum. In theory, this goal can be achieved by delivering the maximum radiation dose to the tumor, while maintaining a zero dose in the surrounding normal tissue. Unfortunately, the physical properties of photons make such a dose distribution virtually impossible. As a result, an optimization procedure is often applied where the maximal dose is given to the tumor and, at the same time, only the minimal dose is allowed for the surrounding healthy tissue.

The *gross tumor volume* (GTV)[1] is the three dimensional space occupied by the gross palpable or visible/demonstrable macroscopic extent of the malignant growth. Unfortunately, malignant tissue can spread on a microscopic scale beyond the visible tumor volume. Hence, the radiation oncologist typically defines a *clinical target volume* (CTV),[1] which is a volume enclosing the GTV and the subclinical microscopic malignant disease. This gap ensures that the dose prescription will cover the entire macroscopic tumor tissue and its microscopic spread. The extent of the margin chosen to accommodate for microscopic spread depends on the tumor type, location, stage, lymphatic expansion, and vascular expansion. Next, a further margin surrounding the CTV is added to the CTV, resulting in a three dimensional volume referred to as: *planning target volume* (PTV).[1] This additional margin is needed to account for geometrical uncertainties attributed to positioning inaccuracies: patient movement, organ movement, respiration, and variation in daily setup. As a result the following two criteria are globally understood as being the pillars of modern radiation treatment planning:

1) Producing a uniform dose distribution within the planning target volume, i.e., minimizing the dose gradient inside the PTV.
2) Minimizing the dose in the surrounding healthy tissue.

The function of the dosimetrist is to produce an optimal dose distribution that fulfills both goals above. Using the patient data in the form of CT images,

simulation films, patient contours, and the CTV (previously defined by the radiation oncologist), the dosimetrist sets off with the purpose of producing the final dose plan with the help of a treatment planning system. The dosimetrist has the following variables to consider: beam modality, beam energy, field size, beam entrance angle, number of beams, beam weights, source-skin distance, and the use of beam modifiers (wedges, blocks, multileaf collimator, compensators, bolus material, ... etc.). These variables can produce a very large number of possibilities, hence the dosimetrist relies on previous knowledge and experience from standard cases of normal geometries in determining the appropriate treatment parameters for a given patient. In difficult or unusual cases the clinical medical physicist in addition to the dosimetrist is often involved in the treatment planning process.

A *treatment planning system* (TPS), which is usually based on a computer platform, is used to determine the final treatment plan. The TPS is capable of producing a visual display (on a screen or on printed paper) of the dose distribution within the patient that would result when a given set of treatment parameters is used. Hence, the TPS takes treatment variables as input, and produces the resulting dose distribution as output by combining the treatment variables with an appropriate set of premeasured physical machine data. The patient data and contour can either be traced and digitized into the TPS computer, or a direct link with the CT scanner can be established to transfer the patient images into the TPS for treatment planning purposes. Treatment planning systems, available commercially, come with various capabilities, e.g., some calculate the dose distribution in two dimensions, while others can perform the calculation and use data from a 3D environment. Speed, convenience, and accuracy depend on a number of software as well as hardware factors implemented in the particular TPS.

Three treatment planning systems are available at the Montreal General Hospital: General Electric Target System (version 4.0), Varian *CADPLAN* Treatment Modeling Workstation (version 2.62), and the McGill Treatment Planning System (version 5.9). The Target System is a two dimensional external beam treatment planning system commercialized by General Electric and based on the original Rad-8 treatment planning system developed by the Digital Equipment Corporation in 1968.[2] The target system provides the option

for either transferring the patient's CT images directly into the TPS or a manual tracing/digitization of the patient's contour and clinical target volume. *CADPLAN*, is a modern three dimensional, CT-based treatment planning system commercialized by Varian. It contains modules for both external beam therapy as well as brachytherapy planning. The McGill Treatment Planning System is a TPS developed at McGill University dedicated for planning of brachytherapy and radiosurgery techniques. The project described in this thesis was primarily involved with the testing and verification of the *CADPLAN* calculation algorithms.

1.4 Motivation for the thesis

In Fig. 1.1 the medical physicist was hardly even mentioned, nevertheless, the role of the medical physicist is very well accepted as a fundamental component for proper patient care in radiotherapy. The physicist is directly involved in the purchase, acceptance, verification, calibration, and maintenance of a large part of the equipment used in radiotherapy. The role of the physicist is clearly outlined in areas such as treatment unit commissioning, calibration, quality assurance, and upgrades.[3,4] The treatment planning stage is a very crucial step in radiation therapy, however, it is difficult to find a well defined procedure for the acceptance, verification and continuous maintenance of treatment planning systems. The literature brings up studies aimed at addressing this problem,[5-12] however, disagreement does exist on fundamental issues, such as the number of verification tests required, test design, acceptance criteria, and application to newly available 3D planning systems.

The work in this thesis will describe the effort afforded by the author for the purpose of establishing a complete program for the verification and quality assurance of a three dimensional external photon beam treatment planning system that was recently installed at the Montreal General Hospital. With the advent of conformal radiation therapy, 3D treatment planning systems are becoming an important component of the treatment process. Conformal radiation therapy can either be two dimensional or three dimensional. In the 2D case, the treatment field is conformed to the two dimensional cross section of the target by using custom made blocks or the multileaf collimator. In 3D conformal therapy, on the other hand, the intensity of the treatment beam is

spacially modulated in addition to conforming the beam to the target cross section. Intensity modulation can be accomplished by using static components such as compensators or by using dynamic components such as a computer controlled multileaf collimator. Our new treatment planning systems allows for 3D planning but not for intensity modulation.

1.5 References

1 International Commission on Radiation Units and Measurements, ICRU Report No. 50. "Prescribing, recording and reporting photon beam therapy" (ICRU, Washington, D.C., 1993).

2 D. W. Cope, R. E. Bentley, and J. Milan, "The use of a PDP-8 computer for on-line treatment planning," in *Computers in Radiology*, Proceedings of International Meeting in Brussels, 157-164 (1969).

3 American Association of Physicists in Medicine Task Group 40, AAPM Report No. 46. "Comprehensive QA for radiation oncology" (American Institute of Physics, New York, 1994).

4 American Association of Physicists in Medicine Task Group 45, AAPM Report No. 47. "AAPM code of practice for radiotherapy accelerators" (American Institute of Physics, New York, 1994).

5 R. G. Dale, "Implementation of the Philips treatment planning system for use in radiation therapy," Br. J. Radiol. **51**, 613-621 (1978).

6 International Commission on Radiation Units and Measurements, ICRU Report No. 42. "Use of computers in external beam radiotherapy procedures with high-energy photons and electrons" (ICRU, Washington, D.C., 1987).

7 J. Jacky and C. P. White, "Testing a 3D radiation therapy planning program," Int. J. Radiat. Oncol. Biol. Phys. **18**, 253-261 (1990).

8 C. Kappas and J. C. Rosenwald, "Quality control of inhomogeneity correction algorithms used in treatment planning systems," Int. J. Radiat. Oncol. Biol. Phys. **32**, 847-858 (1995).

9 A. Kosunen, H. Järvinen, S. Vatnitskij, I. Ermakov, A. Chervjakov, J. Kulmala, M. Pitkänen, T. Väyrynen, and A. Väänänen, "Intercomparison of radiotherapy treatment planning systems for external photon and electron beam dose calculations," Radiother. Oncol. **29**, 327-335 (1993).

[10] M. E. Masterson, G. Barest, C. Chen-Shou, K. Dopke, R. D. Epperson, W. B. Harms, K. E. Krippner, R. Mohan, E. D. Slessinger, M. R. Sontag, M. M. Urie, R. E. Wallace, and J. W. Wong, "Interinstitutional experience in verification of external photon dose calculations," Int. J. Radiat. Oncol. Biol. Phys. **21**, 37-58 (1991).

[11] E. C. McCullough and A. M. Krueger, "Performance evaluation of computerized treatment planning systems for radiotherapy external photon beams," Int. J. Radiat. Oncol. Biol. Phys. **6**, 1599-1605 (1980).

[12] J. Van Dyk, R. B. Barnett, J. E. Cygler, and P. C. Shragge, "Commissioning and quality assurance of treatment planning computers," Int. J. Radiat. Oncol. Biol. Phys. **26**, 261-273 (1993).

Chapter 2:
Principles of Photon Dose Calculation

2.1 Definition of dose in radiotherapy

Dose is defined as the amount of energy absorbed per unit mass of material due to incident ionizing radiation and is expressed in Joules/kilogram. A special SI unit known as the Gray (Gy) was created for use in radiotherapy where 1 Gy is equivalent to 1 J/kg. Mathematically, the dose can be understood best in terms of the energy ε imparted by ionizing radiation to material of volume V and mass m. According to the ICRU,[1] the energy imparted is defined as:

$$\varepsilon = R_{in} - R_{out} + \sum Q, \tag{2.1}$$

where R_{in} is the total radiant energy of charged and uncharged particles entering volume V, R_{out} is the radiant energy exiting volume V, and ΣQ is the sum of changes in all rest mass energies of all particles that might have undergone changes in a nuclear transformation. According to this definition, the imparted energy ε is that part of the transferred energy that remains absorbed within the medium.

The absorbed dose D in volume V is thus given by:

$$D = \frac{d\bar{\varepsilon}}{dm}, \tag{2.2}$$

where $\bar{\varepsilon}$ is a nonstochastic quantity representing the expected or mean value for the imparted energy ε. The mass m has to fulfill the simultaneous requirement of being small in order to provide for the dose at a single point and being large enough to avoid statistical fluctuations due to the stochastic properties of the imparted energy.

2.2 Exposure and its relevance to dose calculation

Dose given by photon beams is primarily delivered by secondary charged particles (electrons) that are set in motion through photon interactions within the irradiated substance. Exposure is one of the oldest and most fundamental quantities used in radiotherapy as it provides a quantitative measure of the ability of radiation to ionize air. Mathematically, exposure X is given by the absolute value of the total charge dQ of ions of one sign produced by incident photons in air of mass dm when all the secondary charged particles are stopped in air:[1]

$$X = \frac{dQ}{dm}. \tag{2.3}$$

The practical unit used for exposure is the Roentgen (R), which is equivalent to 2.58×10^{-4} C/kg of air. By definition, the Roentgen is only applicable to photon beams and cannot be used for other types of radiation. Exposure can only be measured directly using the standard air ionization chamber (also known as the free-air ionization chamber) which is found in

standardization laboratories for the purpose of calibrating thimble ionization chambers. The standard air chamber fulfills the requirement that all secondary charged particles be stopped in air (from the definition of exposure). Under such requirement, *secondary charged particle equilibrium* should exist, where the energies, number and direction of the charged particles are constant throughout the volume of interest.[1] The fulfillment of this prerequisite introduces a practical limitation on the range of energies for which exposure can be defined, limiting the exposure to photon energies below 3 MeV.

In a state of *electronic equilibrium* one can relate the exposure to the dose in air by using the fact that the average energy needed to produce an ion pair in air ($\overline{W}_{air}$) is 33.97 eV/ion pair for dry air.[2] The mean energy required per unit charge produced is then $\overline{W}_{air}/e$ = 33.97 J/C, where e is the charge of an electron. As a result the dose to air is given by:

$$D_{air} = X \cdot (\overline{W}_{air}/e). \tag{2.4}$$

In Eq. (2.4), if the exposure is given in units of Roentgen (R) and the dose to air is calculated in units of cGy (1cGy=10^{-2} Gy), then the quantity ($\overline{W}_{air}/e$) can be written as 0.876 cGy/R. Equation (2.4) then becomes equal to:

$$D_{air}(cGy) = X(R) \cdot 0.876(cGy/R). \tag{2.5}$$

By introducing a small mass of medium Δm into the beam, one is interested in relating the dose to air to the dose received by the medium. The small mass should be large enough to ensure the condition of electronic equilibrium. The following relationship is found to hold:

$$\frac{D_{med}}{D_{air}} = \frac{(\overline{\mu}_{ab}/\rho)_{med}}{(\overline{\mu}_{ab}/\rho)_{air}} \cdot k(r_{med}) = (\overline{\mu}_{ab}/\rho)^{med}_{air} \cdot k(r_{med}), \tag{2.6}$$

where $(\overline{\mu}_{ab}/\rho)$ is the mean mass energy absorption coefficient and $k(r_{med})$ is the transmission factor which accounts for the attenuation of the beam through the radius r of the small mass of medium.

By combining Eq. (2.5) with Eq. (2.6) one can relate the dose to a small mass of medium $D_{\Delta m}$ (also known as the dose in free space) to the exposure as follows:

$$D_{\Delta m}(cGy) = X(R)\cdot\left[0.876(cGy/R)\cdot(\overline{\mu}_{ab}/\rho)_{air}^{med}\right]\cdot k(r_{med})$$
$$= X(R)\cdot f_{med}\cdot k(r_{med}), \qquad (2.7)$$

where f_{med} is referred to as the Roentgen to cGy conversion factor for the absorbing medium.

2.3 Dose distribution within tissue

A dose distribution is the three dimensional description of dose received at any given point in an irradiated material. The dose distribution within the volume of the irradiated medium is usually normalized to the dose at a specific point. By virtue of this normalization it is often sufficient to measure the relative dose within the medium in order to describe the dose distribution. Conventionally, the dose distribution is described by a number of functions which were originally developed to describe the dose in a two dimensional plane: *percentage depth dose*, *beam profile*, and *isodose contours* or *lines*. With the advent of three dimensional treatment planning, *isodose surfaces* were introduced to give a true three dimensional description of the dose distribution.

2.3.1 Percentage depth dose

The central axis percentage depth dose *(PDD)* at point *Q* in phantom is the dose received at that point relative to the dose at a reference point *P* (Fig. 2.1):

$$PDD(d,A,SSD,E) = 100\cdot\frac{D_Q}{D_P}, \qquad (2.8)$$

where *d* is the depth of point *Q* in phantom, *A* is the radiation field size at the phantom surface, *SSD* is the source-skin distance, and *E* is the beam energy.

Notice that both points *P* and *Q* lie on the beam central axis. The point *P* is known as the reference point or normalization point, which is usually chosen

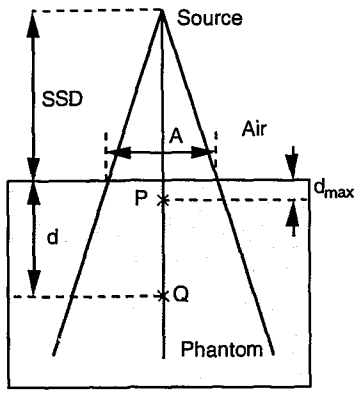

FIG. 2.1. *Schematic representation of the geometrical parameters involved in the definition of percentage depth dose.*

to be the point of maximum dose along the beam central axis with depth denoted as d_{max}. The percentage depth dose function depends on four variables: depth *(d)*, field size *(A)*, source-skin distance *(SSD)*, and beam energy *(E)*. Figure 2.2 shows typical *PDD* distributions for 10 MV and cobalt-60 photon beams in water produced by a 10x10 cm² field at the nominal *SSD* (80 cm for cobalt-60 and 100 cm for 10 MV). Close to the surface there is a build-up region in which the dose rises as the depth increases and peaks at the depth of dose maximum *(d_{max})*. Since the maximum dose does not lie directly on the surface for high energy photon beams, this phenomenon is termed the skin sparing effect. Depth of dose maximum occurs at a depth of 0.5 cm for cobalt-60 beams and 2.5 cm for 10 MV beams. Moreover, d_{max} of megavoltage beams exhibits not only a dependence on beam energy but also on field size.[3] The depth of dose maximum is found to increase rapidly with increasing field size up to a maximum at around 5x5 cm² beyond which d_{max} gradually decreases. However, the field size dependence of d_{max} is generally neglected in radiotherapy with the exception of situations involving extremely small fields (e.g., radiosurgeory) or extremely large fields (e.g., total body irradiation). Since the treatment planning software to be verified in this thesis does not support the

calculation of dose in the buildup region, the verification procedure was concerned exclusively with dose values beyond d_{max}.

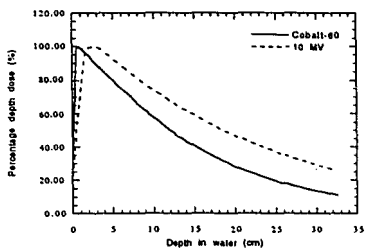

FIG. 2.2. *Percentage depth dose along the beam central axis for both cobalt-60 and 10 MV photon beams in water. Field size was set at 10x10 cm² at the surface of the phantom. The phantom was placed at an 80 cm SSD for cobalt-60 and 100 cm SSD for the 10 MV beam.*

2.3.2 Beam profile

Beam profile describes the dose at a certain depth *d* in phantom along a line perpendicular to the beam central axis. Figure 2.3 illustrates the beam profiles for cobalt-60 and 10 MV beams at a depth of 10 cm in water produced by a 10x10 cm² field at the nominal *SSD*. Beam profile is often used to evaluate the flatness of the photon beam, which is a basic requirement for uniform dose distributions. The flatness of photon beams is defined as the variation of dose relative to the central axis dose over 80% of the field size centered about the beam's central axis at a depth of 10 cm in phantom. This dose variation is expected to be within ± 3% to be considered acceptable for clinical use.[4] The concept of the off-axis ratio (OAR) is very similar to that of the beam profile with the exception that an OAR at a given depth in phantom is represented by the beam profile normalized to 1 at the intersection with the beam central axis.

From Fig. 2.3 one can note that the dose does not simply drop to zero at the geometrical edge of the field. Rather it follows a steep and finite gradient.

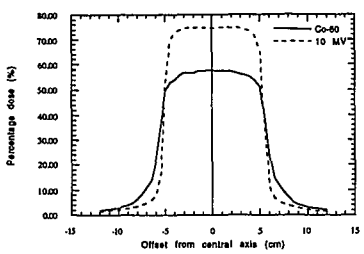

FIG. 2.3. *Lateral beam profile for cobalt-60 and 10 MV photon beams in water at a depth of 10 cm. Field size was set at 10x10 cm² at the surface of the phantom. The phantom was placed at an 80 cm SSD for cobalt-60 and 100 cm SSD for the 10 MV beam. Both profiles were normalized to 100% at the respective depths of dose maximum (d_{max}) on the central axis. The vertical solid line in the middle represents the beam central axis location.*

The term *penumbra,* as defined by the ICRU,[5] is given to the region at the edge of the beam where the dose rate changes rapidly as a function of distance from the beam's central axis. The ICRU further categorizes the penumbra into two parts: geometrical and physical. The geometric penumbra is attributed to thefact that the radiation source is not a point source. Hence the geometric penumbra covers the region in phantom irradiated by primary photons originating from only part of the source. The physical penumbra, on the other hand, is attributed to the contribution of scatter which will be discussed in Section 2.6. The width of the physical penumbra is defined as the lateral distance between two specified *isodose* curves at a specified depth in phantom.[5] The two isodose curves are usually chosen as the 80% and 20% lines or sometimes the 90% and 10% lines.

2.3.3 Isodose lines and isodose surfaces

A central axis percentage depth dose distribution coupled with appropriate beam profiles can describe the dose distribution at any point in a

two dimensional plane in the medium. If one were to join all the points in a plane that receive exactly the same relative dose, then one would be describing an *isodose line*. Isodose lines are considered the most practical visual tool for illustrating the relative dose behavior within a two dimensional plane. Figure 2.4 is a diagram of a typical isodose distribution produced by a 10 MV photon beam for a field of 10x10 cm² at an SSD of 100 cm.

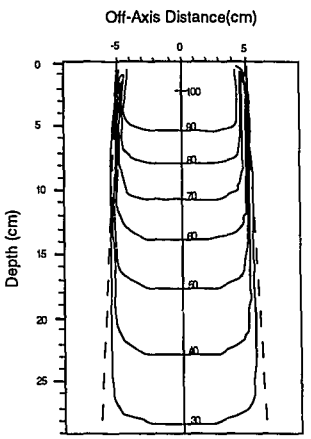

FIG. 2.4. *Isodose lines produced by a 10 MV open photon beam in water. Field size = 10x10 cm², and SSD = 100 cm. All doses are normalized to 100 at the depth of dose maximum on the beam's central axis (d_{max}=2.5 cm).*

One can carry the concept of isodose lines a step further into three dimensions. An *isodose surface* is defined by connecting all points in three dimensions that receive the same relative dose. The use of the full potential of isodose surfaces requires some dynamic visual display capabilities, such as rotation, magnification, displacement, etc. Such capabilities are afforded by today's computers making three dimensional treatment planning an important option in clinical practice.

2.3.4 Dose distribution modification

The shape of the isodose lines can be changed by placing an attenuator, such as a piece of lead, in part of the open beam. This is the main principle governing the modification of dose distribution through altering the spatial intensity profile of the open beam with specially shaped attenuators. Beam modifiers refer to all components that could be used to modify the output or the shape of the field. This definition includes static wedge, dynamic wedge (to be discussed in Section 3.4.2), blocks, compensators, and bolus material. The need for such modifiers stems from the necessity to adjust the isodose line in order to achieve a uniform dose distribution that conforms to a specific geometry defining the irradiated target.

A static or universal wedge is composed of some dense material, such as steel or lead, and has a side profile approximating a triangle. The wedge causes a gradual increase in the attenuation of the beam by proceeding laterally from the thin edge to thick edge (Fig. 2.5). This will cause the isodose lines to tilt according to the angle of the wedge and thereby modifying the dose

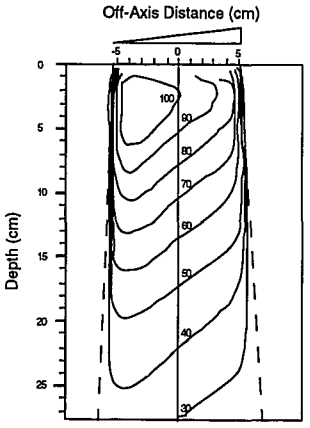

FIG. 2.5. *Isodose lines produced by a 10 MV beam with a 45° wedge in water. Field size = 10x10 cm² and SSD = 100 cm. Doses are normalized to 100 at the depth of dose maximum on the beam's central axis (d_{max}=2.5 cm).*

distribution in the phantom. The wedge angle is defined as the angle separating the isodose line as it intersects the central beam axis from the perpendicular at some reference depth in phantom.[5] A general agreement on the reference depth has not been finalized. Some have decided to use the 50% isodose line[6] to define the wedge angle. This becomes impractical for high energy beams where the intersection of the 50% isodose line with the central axis becomes deeper with increasing beam energy. Therefore the general recommendation is for the use of 10 cm as the reference depth.[5] The placement of the wedge into the beam decreases the dose rate relative to the open beam. The wedge transmission factor is used for absolute dose calculations to account for this effect, and is defined as the ratio of the dose at a reference point on the beam's central axis in phantom with the wedge in place to the dose rate at the same point with only the open field.[5]

Beam blocks are also made of dense material, e.g., lead or cerrobend, and are placed in the beam to shield radiation sensitive organs that otherwise would receive an excessive dose. Hence blocks are custom designed and made for each special case that requires them. The block thickness extends between 5 and 7 half-value layers to provide essentially full primary beam attenuation. However, at the edge of the block a variation of transmission is found because of the decrease of the traversal path of the primary beam. In order to eliminate this problem the side edges of the block may be tapered in such a way as to follow the path of the diverging primary ray.

Human contours hardly ever follow a flat surface as seen in experimental phantoms. As a result compensators or bolus material are used to compensate for missing tissue. Compensators are custom made from sheets of lead or brass mounted on a tray which is placed in the beam at least 20 cm from the patient's skin in order to maintain the skin sparing effect. Bolus, on the other hand, is placed directly on the surface of the patient thereby removing the skin sparing effect of high energy photon beams.

2.4 SSD versus SAD configurations

In clinical cases the dosimetrist usually uses a number of coplanar beams to plan a given treatment. Such multiple coplanar beams can be

arranged in one of two possibilities: an isocentric or SAD (source-axis distance) setup or an SSD setup. In an *SSD setup*, the beams are aimed from different coplanar directions in such a way that the SSD is the same for all beams. This setup makes it easier to calculate the dose distribution by using the percent depth dose (PDD) and beam profiles that were measured at the same SSD. However, the SSD setup is cumbersome in practice since the patient has to be moved for the positioning of every individual beam. In an *isocentric setup*, on the other hand, the machine isocenter is positioned in such a way that it remains in the same relative position with respect to the patient. In such an arrangement the beams needed for the treatment are produced by simply rotating the machine's gantry to the required angle without moving the patient in the process. Although the SAD setup is much more practical, the calculation of dose distributions for this setup is much more difficult because the SSD changes with every beam according to the depth of isocenter in the patient. Hence special functions were introduced to facilitate dose calculations in isocentric setups. These functions are discussed below.

2.5 Additional parameters used in radiotherapy physics

2.5.1 Tissue-air ratio

As shown in Fig. 2.6 the tissue-air ratio (TAR) is defined as the quotient of the dose at point Q in medium (D_Q) over the dose to a small mass of tissue $(D_{\Delta m})$, which was defined earlier in Eq. (2.7):

$$TAR(d, A_Q, E) = \frac{D_Q}{D_{\Delta m}}, \tag{2.9}$$

where d is the depth of point Q in phantom, A_Q is field size as defined at the depth of point Q, and E is the energy of the impinging radiation.

In TAR the field size is defined at the depth of the point Q, in contrast with the PDD field size definition which occurs at the surface of the phantom. Moreover, in Fig. 2.6 the distance from the source to point Q, the source-axis distance (SAD), is equal to the distance to the small mass Δm. A special case of TAR occurs when point Q is at the depth of maximum dose (d_{max}). At this depth TAR is equivalent to the peak scatter factor (PSF). In the literature, the

peak scatter factor (PSF) and back scatter factor (BSF) are used interchangeably. The PSF was developed long before TAR as a factor relating the maximum dose in the medium to the corresponding dose to a small mass in air.

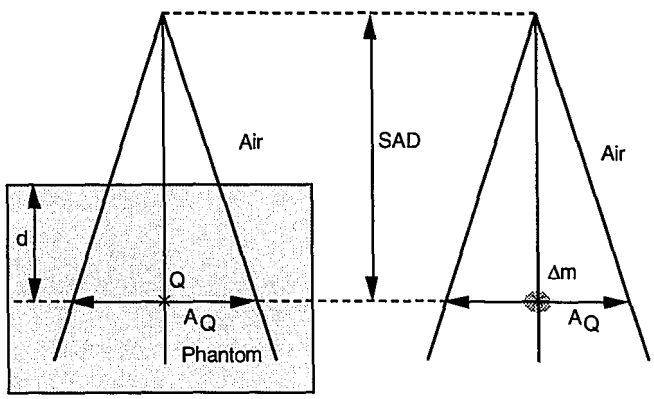

FIG. 2.6. *Schematic representation of the geometrical parameters involved in the definition of tissue-air ratio (TAR).*

The TAR is a very useful tool for isocentric (SAD) treatments because it does not depend on the source-skin distance (SSD). It depends only on the depth in phantom, the field size at SAD, and the energy of the photon beam. However, TAR relies heavily on the definition of exposure and the dose to a small mass of medium, which gives it an application limited to photon energies bellow 3 MeV. Therefore, a further mathematical tool was developed for high energy beams: the tissue-phantom ratio.

2.5.2 Tissue-phantom ratio

As shown in Fig. 2.7 the tissue-phantom ratio (TPR) is defined as the quotient of the dose at point Q in the medium (D_Q) over the dose to point Q_{ref} (D_{Qref}) at a reference depth d_{ref} in the medium:

$$TPR(d, A_Q, E) = \frac{D_Q}{D_{Q_{ref}}}. \tag{2.10}$$

Similarly to TAR, TPR does not depend on the SSD, but depends on the depth in phantom, the field size at SAD, and the photon beam energy. A special case of TPR occurs when the reference point Q_{ref} is chosen at the depth of dose maximum (d_{max}). This special case is used extensively in high energy radiation therapy and is given the term tissue-maximum ratio (TMR). The TMR is defined as follows:

$$TMR(d, A_Q, E) = \frac{D_Q}{D_{Q_{max}}}. \tag{2.11}$$

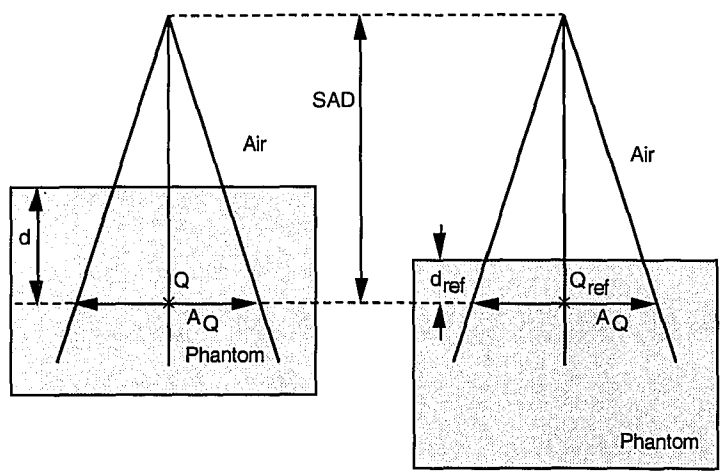

FIG. 2.7. *Schematic representation of the geometrical parameters involved in the definition of tissue-phantom ratio (TPR).*

2.6 *Primary beam and scattered photon contributions*

Due to the physical nature of photon interactions with the absorbing medium, photons scatter (Compton effect) in various directions upon interacting

with matter. As a result an appropriate model is used in photon therapy where the photon beam can be broken into two components: the *primary photon beam* which includes all photons that have not had any interactions with matter and the *scattered photon beam* which includes all scattered photons. In a radiation therapy setting, scattering primarily occurs because of photon interactions in two locations: collimator scattering and in-phantom scattering.

The *collimator factor (CF)*, also known as the collimator scatter factor, represents scattered photons originating from interactions with the treatment unit collimators. Hence, one might expect an increase in the collimator contribution to scattered dose by increasing the field size setting. The collimator factor is defined as the ratio of the dose to a small mass of tissue with a given field size setting of A to the dose to the same small mass but with reference field size setting A_{ref}, which is usually chosen as 10x10cm²:

$$CF(A) = \frac{D_{\Delta m}(A)}{D_{\Delta m}(A_{ref})}. \tag{2.12}$$

The *relative dose factor (RDF)*, also known as the total scatter factor, represents all scattered photons originating from interactions either within the treated medium (phantom) or from collimator interactions. Mathematically RDF is defined as the ratio of the dose to d_{max} in phantom with a given field size setting of A over the dose to the same point in phantom with the field set to A_{ref}, again usually taken as 10x10 cm²:

$$RDF(A) = \frac{D(d_{\max}, A)}{D(d_{\max}, A_{ref})}. \tag{2.13}$$

From Eqs. (2.12) and (2.13) one can derive the phantom *scatter factor (SF)*, which represents the scatter from photon interactions originating only in the phantom, as the ratio of the *RDF* over *CF* at the field size setting of A:

$$SF(A) = \frac{RDF(A)}{CF(A)}. \tag{2.14}$$

2.6.1 Scatter-air ratio

Scatter-air ratio (SAR) is an indirectly measured quantity based on the assumption that the dose in the medium can be considered as the cumulative contribution of a primary beam component and a scatter radiation component. Theoretically SAR can be considered, similarly to the TAR, as the ratio of scattered dose at a point in medium over the dose to a small mass of tissue at the same point. Scatter-air ratio is derived from TAR tables as follows:

$$SAR(d,A,E) = TAR(d,A,E) - TAR(d,0,E), \tag{2.15}$$

where *TAR(d,0,E)* is considered as the primary beam component, i.e., the extrapolated zero field component. The scatter-air ratio is very useful in the calculation of dose distributions for irregularly shaped beams, especially in blocked parts of the beam where there is no primary beam. It has the same properties as *TAR*, in that it depends on the depth in phantom, field size at SAD, as well as, beam energy, and does not depend on the SSD.

2.6.2 Scatter-phantom ratio

Similarly to the SAR derived from the TAR, the *scatter-phantom ratio (SPR)* is the scatter function derived from TPR values. The definition of SPR has been revised since its introduction[7] and is currently accepted as follows:

$$SPR(d,A,E) = TPR(d,A,E) \cdot \frac{SF(A)}{SF(0)} - TPR(d,0,E). \tag{2.16}$$

A special case of the SPR is the *scatter maximum ratio (SMR)* which can be derived using Eq. (2.16) by substituting TMR in place of TPR. As with the SAR, the SMR is used extensively in radiation therapy especially for irregular beam configurations.

2.7 Physical parameters affecting dose distributions

The dose distribution in medium can be affected by various physical parameters related to the photon beam. The most important factors are the

source-skin distance (SSD), field size, and beam energy. The effect of these parameters on the percentage depth dose (PDD) will be presented next.

It is found that the exposure at a point in air varies with the distance from the source according to an inverse square law relationship. However, the *primary* dose in phantom is influenced, not only by the inverse square law, but also by the exponential attenuation of the primary beam in the phantom. Hence one can express the *primary* percent depth dose PDD_p as follows:

$$PDD_P(d,0,SSD,E) = 100 \cdot (\frac{SSD + d_{\max}}{SSD + d})^2 \cdot e^{-(d-d_{\max})\mu}, \qquad (2.17)$$

where μ is the linear attenuation coefficient for the given photon beam energy or spectrum in the phantom material.

From Eq. (2.17) one finds that by increasing the SSD, the inverse square law factor also increases and approaches 1 for very large SSDs, while the exponential attenuation factor is not affected. Even though this only represents the primary component of the dose, this argument can be used to demonstrate that the PDD in general increases with increasing SSD.

The dose in phantom is also affected by the field size, as illustrated in Eq. (2.13) with the relative dose factor which describes the changes in dose at d_{max} with changing field size. Also the PDD is found to increase with increasing field size due to the increased scatter contribution from the phantom and the collimators. However, the amount of this increase depends on the beam energy. In high energy beams the scatter is predominantly in the forward direction which gives the change in field size less of an effect on PDD as compared with low energy beams. The PDD values are normally found tabulated at a number of depths in phantom and also given for a number of field sizes.

The penetrating power of photons in tissue increases with increasing energy due to the decrease in the linear attenuation coefficient μ with energy in the therapeutic range. As a result the PDD (beyond d_{max}) increases with an increase of the beam effective energy. Furthermore, the depth of d_{max}

increases with increasing beam energy. This makes the skin sparing effect more profound for high energy radiation and thereby improving the possibility of delivering high dose values to deep tumor locations.

2.8 Summary

In this Chapter the fundamental concepts relevant to radiation treatment planning were presented. The points discussed covered basic radiotherapy physics items, such as dose, exposure, and dose distribution, that will be referred to frequently in the next chapters. The difference between SAD and SSD treatment techniques was discussed and the basic functions (PDD, OAR, TAR, TPR, SAR and SPR) used in describing dose distributions in treatment planning were presented. Physical parameters affecting the dose distribution were also illustrated.

2.9 References

1 International Commission on Radiation Units and Measurements, ICRU Report No. 33. "Radiation quantities and units" (ICRU, Washington, D.C.,1980).

2 M. Boutillon and A. M. Perroche-Roux, "Re-evaluation of the W value for electrons in dry air," Phys. Med. Biol. **32**, 213-219 (1987).

3 K. E. Sixel and E. B. Podgorsak, "Buildup region and depth of dose maximum of megavoltage x-ray beams," Med. Phys. **21**, 411-416 (1994).

4 National Council on Radiation Protection and Measurements, NCRP Report No. 69. "Dosimetry of x-ray and gamma ray beams for radiation therapy in the energy range of 10 keV to 50 MeV" (NCRP, Bethesda, MD, 1981).

5 International Commission on Radiation Units and Measurements, ICRU Report No. 24. "Determination of absorbed dose in a patient irradiated by beams of x or gamma rays in radiotherapy procedures" (ICRU, Washington, D.C., 1976).

6 H. E. Johns and J. R. Cunningham, *The Physics of Radiology*, 4th ed. (Charles Thomas, Springfield, IL, 1983).

7 F. M. Khan, W. Sewchand, J. Lee, and J. F. Williamson, "Revision of tissue-maximum ratio and scatter-maximum ratio concepts for cobalt 60 and higher energy x-ray beams," Med. Phys. **7**, 230-237 (1980).

Chapter 3:
Treatment Planning Systems

3.1 Computerized treatment planning systems

The introduction of computers into radiotherapy has greatly improved the radiotherapeutic process in terms of efficiency, speed, reproducibility, and accuracy. Prior to the computer technology all treatment planning was done manually. The dosimetrist would transcribe the patient contour onto paper and, upon deciding on the treatment parameters and field configuration, the dose distribution would be traced by hand for standard phantom geometries and then corrected for the irregular patient contour by shifting the isodose lines. Not only was this process very consuming in terms of man-power, it also meant that any possible correction or optimization of treatment plans corresponded to a huge expenditure of energy and time.

Original efforts in the field of computerized treatment planning go as far back as the early 1960s when Bentley[1] laid the first foundation for a computerized treatment planning algorithm. The first commercial treatment planning system was the RAD-8, developed by the Digital Equipment

Corporation in 1968.[2] This was immediately followed by the programmed console (PC) in 1969, designed and developed at Washington University, St. Louis, U.S.A.[3,4] Further down the line, the combined effort of Milan and Bentley[5] produced a formidable data storage and manipulation scheme which is still being implemented in many treatment planning systems produced today (see next section). This step was very crucial at a time when data storage and manipulation was limited by scarce resources of computer memory (Table 3.1). The contributions of Jack Cunningham to the area of treatment planning should also be aknowledged. While in Toronto, Cunningham developed his own treatment planning software for use on inhouse computer systems. The software was later developed and marketed first by AECL, Ottawa, as the TP-11 treatment planning system, and later by Theratronics, Ottawa, as the Theraplan treatment planning system. A 3D version of Theraplan is to be released by Theratronics as Theraplan-Plus in the Fall of 1996.

TABLE 3.1. *A concise chronological overview of advancements in computerized treatment planning.*

Advancement	Year
First Treatment Planning Algorithm (Bentley)[1]	1964
First Commercial TPS	
RAD-8 [2]	1968
Programmed Console (PC)[3,4]	1969
Data Storage and Manipulation (Milan and Bentley)[5]	1974
Increase in computer speed and memory Increased interactive ability	1980s
3D Treatment planning Dynamic beam manipulation	1990s

During the 1980s, a number of planning systems were produced that exploited the expanding computer technology, especially hardware capability, in improving the speed of data manipulation, and expanding the data storage ability of the existing treatment planning algorithms. This decade can be

characterized by the huge jump in the interactive ability between the planning system and the user. The 1990s continued along the same line by using a rapidly growing computer technology, which is continually improving in cost effectiveness. Furthermore, this decade can be characterized by an increased demand in the areas of three dimensional treatment planning, as well as in the dynamic beam manipulation.

3.2 Dose calculation algorithms

A computerized treatment planning system for external beam therapy consists of a mathematical model used to describe an external beam. This mathematical model is then implemented by various computer programs and algorithms to describe various complex treatment geometries. This section provides the basic principles of the major algorithms developed for the purpose of treatment planning. It is not intended to include *all* such algorithms developed to date.

Milan-Bentley[5] data storage and manipulation algorithm. In general, in order to determine the dose distribution in the central axis plane, one needs to have the dose values for an overlying two dimensional grid. As a result a TPS would require such a grid for every field size (width and length) in order to generate an arbitrary treatment plan. Unfortunately, in the early days of computing, such large beam data corresponded to a very valuable memory block and a large time expenditure in measuring such data. A more feasible alternative was to consider the dose at any point in the central axis plane as a product of the central axis percentage depth dose (PDD), and the corresponding off-axis-ratio (OAR), as follows:

$$Dose(x,z) = PDD(z) \cdot OAR(x,z), \tag{3.1}$$

where x is the distance from the central axis and z is the depth of the point in the medium.

Milan and Bentley proposed that the set of beam data need only be composed of central axis depth dose measurements and of off-axis-ratio measurements (at five different depths) for a series of square fields. This

resulted in a more efficient use of computer memory and calculation time. For points that lie at depths between the measured beam profiles, the dose can be found by a linear interpolation along diverging fan lines. Sterling's[6] approximation was implemented for rectangular fields, where the side of the equivalent square *a* is approximated by the equation:

$$a = \frac{2F_x \cdot F_y}{(F_x + F_y)}, \tag{3.2}$$

with F_x and F_y the field width and field length, respectively.

Beam generating function.[7] The development of such a function is considered an extension to the Milan-Bentley data storage format. This method is intended for the purpose of finding the dose in the medium using an analytic function rather than numerically stored data. The beam generating function is found by fitting the coefficients of an analytical expression to the beam data. Hence, such algorithms attempt to fit a function to the percentage depth dose data and another function to the beam profile data. Most of such curve fitting algorithms were produced on mere empirical observations. They provide a convenient way to represent the treatment beam, with very little demand on memory storage. Nevertheless, all such analytic formulas suffer from inherent limitations on the number of geometries where the dose distribution could be calculated with an acceptable uncertainty.

Separation of primary and scatter radiation. This method describes the dose at a given point in phantom as the sum of a primary dose due to the primary incident beam and a scatter dose due to the contribution of radiation that has undergone a scattering process (see section 2.6), as follows:

$$D(x,y,z) = D_p(x,y,z) + D_s(x,y,z), \tag{3.3}$$

where $D_p(x,y,z)$ is the primary component of dose at point (x,y,z) and $D_s(x,y,z)$ is the secondary component.

Johns and Cunningham[7,8] proposed the scatter-air ratio (SAR) as a quantitiy to describe the scatter dose. The scatter-air ratio was derived from

tissue-air ratio (TAR) as described in section 2.6.1, while the zero area field TAR was used to describe the primary beam component.

The pencil beam convolution model[7] is based on the principle that the dose $D(x,y,z)$ at any point (x,y,z) in the phantom can be expressed as a convolution between a point spread function (also known as pencil beam or convolution kernel) and a beam intensity distribution (also referred to as photon fluence distribution):

$$\begin{aligned} D(x,y,z) &= K(x,y,z) * \phi(x,y,z) \\ &= \iiint \phi(x',y',z') \cdot K(x-x',y-y',z-z')\,dx'\,dy'\,dz', \end{aligned} \tag{3.4}$$

where $K(x,y,z)$ is the pencil beam kernel and $\phi(x,y,z)$ is the beam intensity function.

The computational convenience of the convolution model is the fact that the integral in Eq. (3.4) can be evaluated by a direct multiplication of the corresponding Fourier transforms of the two functions. Increasing demands and applications from other fields, e.g., data analysis and imaging, have fueled great advances in the field of Fourier transform computation, making the pencil beam convolution model very attractive. The beam intensity function ϕ is a two dimensional matrix whose entries represent the beam intensity in a plane perpendicular to the beam axis. The determination of the pencil beam function might be the most challenging and controversial step when using the convolution model. Often, the derivation process of the pencil beam functions from the beam data is guarded under high secrecy, especially when such a process is implemented in a commercial TPS.

Monte Carlo simulation. In theory, the best approach to calculating the dose distribution is from first physical principles. This is done by following the history of a photon (and any secondary charged particles it might produce) within the medium, using the first principles of photon interactions with matter (photoelectric, Compton, and pair production interactions). However, the deposition of dose and energy in matter is a highly statistical process. As a result, one needs to follow a very large number of such photons and secondary particles in order to arrive at a statistically significant representation of the dose

distribution.[8] Monte Carlo methods provide a very powerful calculation tool for any possible treatment geometry. The drawback to this process is the huge computational power that is needed to produce a dose distribution within a reasonable amount of time. This technique has yet to be implemented commercially in treatment planning, even though the calculation times required to produce a typical dose distribution have fallen considerably during the past few years.

3.3 Three dimensional treatment planning

The field of treatment planning has historically evolved in two dimensional space because of the inherent two dimensional characteristics of conventional dose modeling. In their original form, the following functions were limited to two or less spatial dimensions: percentage depth dose (PDD), off-axis-ratio (OAR), tissue air ratio (TAR), tissue phantom ratio (TPR), scatter function (SF), scatter air ratio (SAR), and scatter phantom ratio (SPR). As a result, the dose calculation was limited to the display plane, which is often a transverse cross section through the patient. Later-on pseudo-3D systems were developed incorporating some information from the third dimension in their dose calculation. This is especially true in the definition of field size, i.e., the dose distribution due to a 10x5 cm^2 field is different from that for a 10x10 cm^2, for example. Nevertheless, such systems are still considered pseudo-3D, or even only 2D, because of the inherent assumption in the dose calculation that the patient's shape is a "cylinder" whose cross-section projection produces the two dimensional transverse plane (Fig. 3.1).

In principle, a treatment planning system can be characterized as three dimensional, if it meets the criterion of incorporating three dimensional patient data in the final calculation of the dose distribution. Further advances in computer software as well as hardware technologies have added other essential characteristics expected of 3D TPS which were only considered optional a few years ago. These characteristics include: the ability to use CT images in the process of treatment planning, full support of non-coplanar beam geometry, support for *Beam's Eye View* (BEV) display or any variation thereof, e.g., Physician's Eye View (PEV), as well as an inhomogeneity correction algorithm incorporating three dimensional patient information.

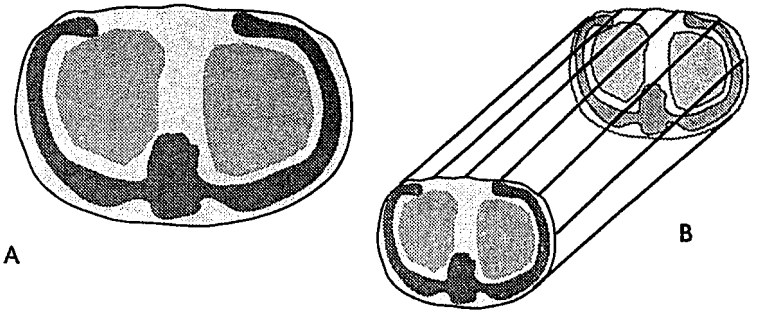

FIG. 3.1. **A** *Transverse plane through the patient in the thorax area.* **B** *The representation of the patient in a pseudo 3D TPS, as used in pseudo 3D dose distribution calculations.*

As appropriately indicated in a study done by the *Photon Treatment Planning Collaborative Working Group*,[9] a state-of-the-art three dimensional TPS should fulfill a number of strict criteria, which, in addition to the general abilities of a 2D system, should include the following provisions:

1) *Patient data transfer.* This can be accomplished best by using a direct ethernet connection from the CT scanner to the TPS. Other forms of data transfer would basically use a data storage medium as the data carrier, e.g., magnetic tape, optical disk, floppy disk, etc. The latter option is definitely more labor intensive when it comes to data transfer, but serves well for the purpose of data archiving.

2) *Patient data manipulation.* The TPS should provide provisions for outlining of structures, such as the planning target volume and critical organs. The task can be accomplished by either manual delineation of organs or automatic contouring. The first option is very time consuming, while the second option is still prone to programming errors. The ability to select freely single or multiple CT slices, to add and delete, and also to limit the calculation to a certain range of slices can be of great convenience. The availability of a high

quality display for CT images with means to change the window level and window width is an essential prerequisite for this step.

3) *Interactive ability.* Any computer-based program is expected to achieve a certain level of interactive ability in its user interface. On one hand, a low level of interactive capability would introduce serious limitations on the operator, while, on the other hand, a high level of interactive capability would correspond to an increased freedom, which would also render the TPS program vulnerable to human errors with possibly serious consequences. As a result, a careful balancing act is essential in the TPS design.

4) *Alternative patient perspective.* The most common display is the beam's eye view (BEV). Beam's eye view is an alternative display perspective, which represents to the operator the patient's structures as seen from the position of the radiation source inside the treatment unit. BEV is a very strong and convenient way to modify fields, especially when combined with the ability to outline blocks and beam apertures interactively in the BEV display.

5) *Conformal therapy.* Conformal therapy is becoming increasingly attractive to physicians especially with the widespread popularity of multileaf collimators. The ability to plan for conformal therapy should include both the multileaf collimator support as well as dynamic intensity modulation of the therapeutic beam. This support should cover both static and rotational beams, planar and non-coplanar.

6) *Stereotactic radiosurgery.* Although stereotactic radiosurgery can be considered as a form of conformal therapy, it is such a specialized treatment modality that it warrants individual attention and specialized dedicated treatment planning approaches.

7) *Plan comparison and evaluation.* Provisions should be available for a qualitative as well as a quantitative comparison among different treatment plans. Dose volume histograms (DVH) are proving to be a valuable tool in 3D plan evaluation since they compress hard-to-visualize three dimensional information into a an easy to understand two dimensional graph. An option to simultaneously display multiple plans is still a very popular qualitative tool.

8) *Treatment verification.* Treatment verification can be achieved virtually by producing projections of the beams onto a digitally reconstructed radiograph (DRR), in essence a virtual portal image.

9) *Quantitative analysis of biological dose distribution.*[10] The use of a computerized algorithm that would evaluate the effects of radiation on the different biological tissues can provide an analytical tool in the quantitative evaluation of treatment plans. Among the proposed parameters for such an algorithm are the dose volume histograms (DVH), normal tissue complication probability (NTCP), and tumor control probability (TCP).

10) Although *automatic optimization* of treatment plans is still under development, it is expected that optimization ability will most likely join the list above as a very important member in the foreseeable future.

3.4 CADPLAN

3.4.1 Dose calculation ability

CADPLAN External Beam Modeling, version 2.62 (from here-on referred to as either *CADPLAN* Treatment Planning System (CTPS), or simply *CADPLAN*) is an extensive computerized treatment planning system for external photon beam therapy offered commercially by Varian Associates (Palo Alto, California). It is capable of handling treatment geometries ranging from the very basic to the most complicated. In radiation therapy there are many parameters that can influence the dose calculation. Such parameters can be grouped into two main categories: physical, i.e., those associated with the treatment beam and clinical, i.e., those associated with the treated patient. CTPS is able to generate dose plans allowing for all the possible permutations of both beam and patient parameters.

On the one hand, the treatment beam parameters include: energy, field shape, beam modifiers, number of beams, beam weighting, SSD vs. SAD setup, or even moving beams. In CTPS the field could take on various geometries: square, rectangular, circular, or irregular. The field shapes can be categorized into either symmetric or asymmetric fields. Asymmetric field treatment is becoming more important with the increased availability of

asymmetric jaws in linacs. Multiple beams can be incorporated into the treatment plan in the *CADPLAN* calculation. These beams can take on various weights to optimize the dose distribution. They could be arranged in an SSD or SAD setup, in coplanar or non-coplanar geometry. Moving beams, such as arc and rotation therapy, can also be selected. Furthermore, CTPS has the ability of computing the number of monitor units (for linear accelerators) or treatment times (for cobalt-60 units) for each individual beam needed to deliver a certain dose prescription.

On the other hand, the patient/treated medium parameters include the contour of the medium and embedded inhomogeneities. The CTPS calculation algorithm includes provisions to correct for both of these factors. Moreover, the CTPS provides an interface to a CT scanner for direct transfer of patient CT images; this is important for the identification of medium inhomogeneities, which is accomplished by automatically converting the CT numbers to the corresponding relative electron densities. *CADPLAN* is not limited to external photon beam modeling; it is also capable of producing dose plans for electron beams as well as for brachytherapy techniques.

3.4.2 Configuration

The configuration of the *CADPLAN*[11] software involves various steps for photon treatment at which a number of beam data as well as treatment machine data are entered. This information can be entered by one of three ways: a) manual table entry through the keyboard, b) digitized from a plot, c) in digital form, i.e., in a data file arranged in the appropriate format. The beam data is stored in *CADPLAN* following the Milan-Bentley[5] storage format as outlined in Section 3.2. Some configuration steps involve calculations of relevant tables and variables, and such calculations are performed automatically by the CTPS.

a) Open Fields: External beam modeling in *CADPLAN* depends on beam data in the form of percentage depth doses and beam profiles. This data is measured for *square* fields , and square fields only, ranging in size from the minimum to the maximum field size. Percentage depth doses (PDDs) are needed for every photon energy and field size; the CTPS has the ability to interpolate PDD data for missing field sizes. Beam profiles at five different

depths are required (e.g., at d_{max}, 5, 10, 15, 20, and 25 cm). The profile curves should be given along the field lateral axis, while extending at least 4 cm outside the geometrical boundary of the field. The profile data should be given at the same depths for all field sizes. It is important to note that a measured open beam profile, as part of the beam data, covers only half the field. This is due to *CADPLAN's* implied assumption that an open beam profile is perfectly symmetric.

In our department, the CTPS was supplied with central axis PDDs for open fields at the nominal SSD distance, as well as with open beam half profiles. The five beam half profiles were given at depths of 2.5, 10.5, 18.5, 26.5, and 34.5 cm for the Clinac-18 10 MV beam, and depths of 0.5, 8.5, 16.5, 24.5, and 32.5 for the cobalt-60 photon beam. Table 3.2 summarizes the measured beam data provided for the two treatment machines.

b) Wedged Fields: Similarly to open fields, wedged fields require beam data in the form of PDDs and lateral beam profiles for *square* fields. PDD curves are needed for every energy, field size, and wedge angle. Lateral beam profiles should be given at the same depths as those entered for open fields. The same field sizes are used for open and wedged fields. While open field profiles cover only half the field, wedged field lateral profiles extend to both sides of the square field. Furthermore, in addition to the 5 lateral profiles, a longitudinal profile measured for only half the field at a depth of 5 cm is required. This profile is assumed symmetric and is used to account for the beam hardening effects introduced when using wedges as beam modifiers.

For wedged fields, PDDs and beam profiles were entered for every beam angle used with the particular machine at the nominal SSD distance (Table 3.2). Note that the wedge beam profiles are measured at the same depth as those used for open beams.

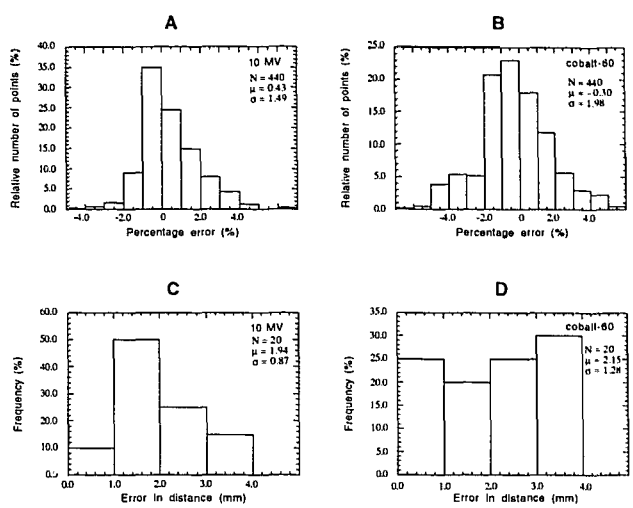

FIG. 5.10. *The error histogram for the multiple beam configuration. Each histogram includes data points from both setups: SSD and SAD. Parts* ***A*** *and* ***B*** *display the percentage error histogram for the 10 MV beam and the cobalt-60 beam, respectively. Parts* ***C*** *and* ***D*** *illustrate the positioning error in locating the 50% point in the penumbra region for the 10 MV and the cobalt-60 beams, respectively. The total number of points N, mean value* μ *and standard deviation* σ *of the error are also indicated for each histogram.*

5.2.5 Moving fields

Moving fields in the form of arc or rotational therapy beams deliver dose in the treated material by rotating the gantry of the treatment unit about the isocenter during the beam "ON" time. In rotational therapy the gantry undergoes a full revolution while in arc therapy the gantry rotation is limited to a preselected angle describing the extent of the arc. The moving fields test is aimed at studying the dose distribution calculated by *CADPLAN* for arc therapy and comparing it with an experimentally measured distribution.

Thermoluminescent dosimeters (TLDs) were used for experimental measurements in this test. A cylindirical phantom with a radius of 15 cm was used. The phantom is made from white polystyrene and is composed of four 3-cm-thick slabs. The TLDs were placed in a 6 mm thick slab that was centered about the central axis plane. Two cases of arc therapy were selected for this test. Both cases had an arc defining an angle of 180° spanning the anterior half of a full rotation. However, in the first case a 5x5 cm^2 field (defined at the isocenter) was used; the machine isocenter was placed directly at the center of the cylindrical phantom. For the second case a 10x10 cm^2 field (also defined at the isocenter) was used but the isocenter was displaced by 5 cm radially from the phantom's center toward the anterior direction. For both cases the verification points were measured along the radial PDD placed symmetrically at the center of the 180° arc. The relative dose distribution was normalized to 100% at the isocenter. The comparison results are given in Fig. 5.11.

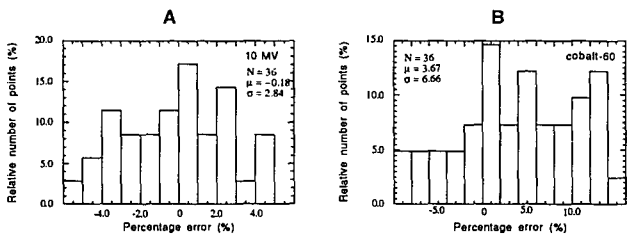

FIG. 5.11. *The error histogram for the moving field configuration. Each histogram includes data points from the two arc therapy cases. Parts* ***A*** *and* ***B*** *display the percentage error histogram for the 10 MV beam and the cobalt-60 beam, respectively. The total number of points N, mean value* μ *and standard deviation* σ *of the error are also indicated for each histogram.*

Figure 5.11 (B) illustrates a significant disagreement between measured and calculated relative dose for the cobalt-60 beam. Further analysis has pointed to a significant variation in the gantry rotation speed of the T-780 cobalt unit. It was noticed that the gantry rotation speed can be as much as 14% slower during an up-swing as compared to a down-swing. The variation of gantry speed would change the beam weight from different angles along the arc which is bound to affect the measured dose distribution. On the other hand, this problem is not found with the Clinac-18 linac. For the linear accelerator, the

operator defines the number of monitor units delivered per each degree of gantry rotation. So using a feed back loop from the monitor chamber, the gantry will only rotate when the number of MUs for the previous angle have been completed. Figure 5.11 (A) shows a good agreement for Clinac-18 10 MV beam, where more than 80% of the points were within ±4%. The experiment with the cobalt-60 arc rotation clearly showed that arc therapy with our cobalt-60 unit should be used with care and that proper treatment planning should account for the variations in gantry rotation speed.

5.3 Monitor unit and treatment time calculation

Although it is more prudent to carry out monitor unit and treatment time calculations manually (which is the policy adopted by our department), *CADPLAN's* calculation of monitor unit settings (for the 10 MV beam) and treatment time (for the cobalt-60 beam) were verified, nevertheless, for the sake of completeness. The manual calculations were carried out according to the acceptable standards found in the literature.[8,9] The results were compared with *CADPLAN's* calculations and are summarized in Table 5.1, below.

The test cases were taken from those investigated earlier in the previous sections. With the exception of the irregular field, the multiple beam SAD setup, and arc fields, all dose distributions for the test cases were normalized to 100% at point of dose maximum on the central beam axis. The SAD and arc field cases were both normalized to 100% at the isocenter, while the blocked field was normalized to 100% at the maximum dose on the central axis of the open beam collimator setting. Moreover, the treatment time calculations performed for the cobalt beam took into account the exponential source decay and the unit's shutter error (+0.02 min). The results from *CADPLAN's* calculation agreed well with the manual calculations with the exception of the SAD case. In order to calculate the treatment time for the SAD case an accurate knowledge of the tissue-maximum ratio (TMR) is required. *CADPLAN* estimates the value of TAR/TPR from entered beam data. A further investigation into the TMR estimate was carried out where the SAD plan was normalized according to a TMR weighting. Under those conditions the value at the isocentre should correspond to the sum of TMR values for each of the individual beams. Upon comparison of the value at the isocenter with the tabulated TMR values a discrepancy of 1.8%

TABLE 5.1. *Comparison of monitor unit and treatment time calculations between manual methods and CADPLAN's algorithm.*

Test Cases	10 MV (MU)		cobalt-60 (min)	
	CADPLAN	Manual	*CADPLAN*	Manual
Standard Geometry				
•Square Field				
10x10 cm^2 at the nominal SSD	250	250	3.08	3.08
•Rectangular Field				
10x30 cm^2 at the nominal SSD	245	243	2.97	2.95
•Change in SSD				
10x10 cm^2 at (nominal -20 cm)	160	160	1.70	1.69
•Wedged Field				
10x10 cm^2 with 45° wedge	368	368	7.10	7.09
Complex Geometry				
•Oblique incidence 60				
10x10 cm^2 at nominal SSD	250	250	3.08	3.08
•Partial Volume Irradiation				
10x10 cm^2 at nominal SSD	252	252	3.10	3.10
•Irregular Field				
15x15cm^2, 5x5cm^2 corner block	248	250	3.05	3.07
•Multiple Beams				
SSD setup				
Beam 1 (weight=0.74)	185	185	2.28	2.28
Beam 2 (weight=1)	250	250	3.08	3.08
•SAD setup				
Beam 1 (weight=0.5)	158	162	4.33	4.31
Beam 2 (weight=1)	316	324	8.67	8.60
•Arc Therapy				
Case 2	293	293	4.67	4.63

was observed for the 10 MV beam and 1.0% for the cobalt-60 beam. It is apparent that *CADPLAN's* estimate of TMR value is not sufficiently accurate and should account for the error seen in Table 5.1. Therefore, it is a wise suggestion to verify always using an independent method the monitor unit and treatment time setting calculated with the treatment planning system.

5.4 Summary

In this Chapter an extensive dose distribution verification scheme was presented. The dose distribution verification covered standard and complex treatment geometries. Results were given for each individual testing configuration. The calculation algorithm of *CADPLAN* was found to be in agreement with measured dose distributions for the standard geometry case. Very good agreement was also observed for the complex geometries. However, shortcommings were observed for the partial volume irradiation and irregular field cases and were indicated in each respective section. Moreover, the monitor unit and treatment time calculation of the treatment planning system was also verified for each individual testing configuration and the results were presented (Table 5.1).

5.5 References

1 J. Milan and R. E. Bentley, "The storage and manipulation of radiation dose data in a small digital computer," Br. J. Radiol. **47**, 115-121 (1974).

2 International Commission on Radiation Units and Measurements, ICRU Report No. 42. "Use of computers in external beam radiotherapy procedures with high-energy photons and electrons" (ICRU, Washington, D.C., 1987).

3 American Association of Physicists in Medicine Task Group 23, AAPM Report No. 55. "Radiation treatment planning dosimetry verification", (American Institute of Physics, New York, 1995).

4 *RFA 300 radiation field analyzer, operation manual* (Scanditronix AB, Uppsala, Sweden, 1992).

5 J. Van Dyk, R. B. Barnett, J. E. Cygler, and P. C. Shragge, "Commissioning and quality assurance of treatment planning computers," Int. J. Radiat. Oncol. Biol. Phys. **26**, 261-273 (1993).

[6] E. B. Podgorsak, M. Gosselin, M. Pla, T. H. Kim, and C. R. Freeman, "A simple isocentric technique for irradiation of the breast, chest wall and peripheral lymphatics," Br. J. Radiol. **57**, 57-63 (1984).

[7] E. B. Podgorsak, M. Pla, M. Gosselin, J. F. Guerra, and C. R. Freeman, "The McGill isocentric breast irradiation technique," Medical Dosimetry **12**, 3-7 (1987).

[8] H. E. Johns and J. R. Cunningham, *The Physics of Radiology*, 4th ed. (Charles Thomas, Springfield, IL, 1983).

[9] F. M. Khan, *The Physics of Radiotherapy*, 2nd ed. (Williams & Wilkins, Baltimore, MD, 1994).

Chapter 6:
Inhomogeneity Correction

6.1 Inhomogeneity correction methods

Without the use of inhomogeneity corrections the dose distributions are calculated with the assumption of a homogeneous medium composed of water or soft tissue. Unfortunately the presence of different tissues with varying radiological properties, e.g., lung, bone, fat, and muscle make such an assumption inaccurate. The level of inaccuracy introduced by ignoring the inhomogeneity correction can be as large as 20% for regions such as the chest containing the lungs.[1]

The presence of an inhomogeneity in an otherwise homogeneous phantom will affect the photon beam dose distribution in the following fashion:

a) *Changes in the primary beam.* The inhomogeneity will attenuate the primary beam in a different manner than does water or soft tissue. This effect is most evident for points located beyond the inhomogeneity.

b) *Changes in the pattern of scattered photons.* Not only does the inhomogeneity affect the attenuation of the primary beam, it also affects the pattern of scattered photons. Points that are beyond the inhomogeneity and are relatively close to it are affected by the changes in the primary beam as well as the changes in the scattered photons.

c) *Changes in secondary charged particle (electron) fluence.* Changes to the electron fluence will primarily affect points located within the inhomogeneity and at its boundaries.

The Compton effect is the predominant mode of interaction for therapeutic beams in the megavoltage range. Compton interactions are primarily dependent on the volumetric electron density (number of electrons per unit volume) of the irradiated medium. Therefore most inhomogeneity correction methods use the volumetric electron density (or relative electron density ρ_e which is the volumetric electron density of the inhomogeneity relative to the volumetric electron density of water) as an important parameter in the calculation of the correction factor. In this work we will refer to the relative volumetric electron density simply by relative electron density ρ_e. Any reference to a mass electron density (number of electrons per unit mass) will be indicated as it occurs.

CADPLAN offers the choice of three inhomogeneity correction algorithms that can be used for treatment planning. Two of these algorithms are based on the concept of effective path-length, namely the *generalized Batho power law* and the *modified Batho power law.* Algorithms based on effective path length use the corresponding relative electron densities of inhomogeneities found along a diverging fan line connecting the point of calculation to the radiation source in order to calculate the effective path length through water. In addition to the two effective path-length algorithms, a third algorithm is available under the name of *equivalent tissue-air ratio* (ETAR). This algorithm was designed for CT pixel-based calculation that uses three dimensional patient or phantom information.

6.1.1 The Batho power law methods

The Batho power law was first introduced by Batho[2] in 1964 as an extension to the tissue-air-ratio method. In its original form the Batho power law was designed to calculate the correction factor for points beyond a single lung inhomogeneity as shown in Fig. 6.1, and can be written as:

$$C_i = \left\{ \frac{TAR(d_3, A_Q)}{TAR(d_2, A_Q)} \right\}^{1-\rho_e}, \tag{6.1}$$

where C_i is the inhomogeneity correction factor, d_3 is the distance from the point of interest Q to the lower surface of the inhomogeneity, d_2 is the distance from point Q to the upper surface of the inhomogeneity, and ρ_e is the relative electron density of the inhomogeneity (Fig. 6.1).

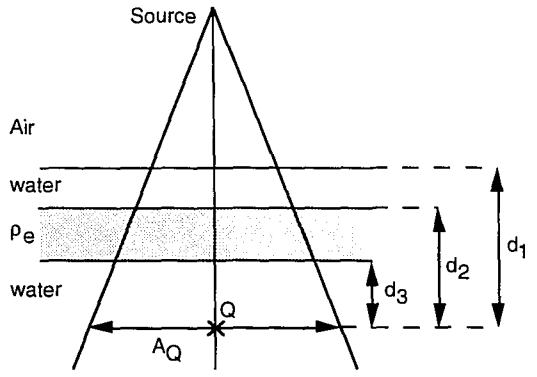

FIG. 6.1. *Schematic diagram of the parameters used for inhomogeneity correction using the Batho power law. The diagram illustrates a flat slab of inhomogeneity with relative electron density ρ_e inserted into a standard water phantom.*

The original power law was further improved to a more general form by Sontag and Cunningham[3] where corrections for points *within* as well as beyond a single inhomogeneity can be calculated by:

$$C_i = \frac{TAR(d_1, A_Q)^{(\rho_e)_1-(\rho_e)_2}}{TAR(d_2, A_Q)^{1-(\rho_e)_2}} \cdot K, \qquad (6.2)$$

where $(\rho_e)_1$ is the relative electron density of the material at the point of calculation Q, d_1 is the distance from point Q to the lower surface of the overlying material, $(\rho_e)_2$ is the relative electron density of overlying material, d_2 is the distance from Q to the upper surface of the overlying material, A_Q is field size at point Q, and K is the ratio of mass energy absorption coefficient of material $(\rho_e)_1$ over the mass energy absorption coefficient of material $(\rho_e)_2$, i.e., $K = (\mu_{ab}/\rho)_{(\rho_e)_1} / (\mu_{ab}/\rho)_{(\rho_e)_2}$.

However, the power law as it stands in Eq. (6.2) has a limited application to phantoms containing only a single inhomogeneity. Furthermore, the correction factor does not take into account the distance from the calculation point Q to the surface of the phantom (d_1 in Fig. 6.1). Webb and Fox[4] have adapted Eq. (6.2) to the currently recognized form of the generalized Batho power law and allowed it to handle multiple layers and multiple inhomogeneities. Cassell et al.[5] showed that one can implement the generalized power law in CT based treatment planning systems in the following form:

$$C_i = K_N \prod_{m=1}^{N} TAR(d_m, A_Q)^{(\rho_e)_m-(\rho_e)_{m-1}}, \qquad (6.3)$$

where m is the index for inhomogeneity boundaries (m=0 corresponds to water), d_m is the distance between the point of calculation Q and the m-th inhomogeneity upper boundary, $(\rho_e)_m$ is the m-th inhomogeneity relative electron density, and K_N is defined as in Eq. (6.2) as follows:

$$K = (\mu_{ab}/\rho)_N / (\mu_{ab}/\rho)_0 = (\rho_{el})_N, \qquad (6.4)$$

where $(\mu_{ab}/\rho)_N$ and $(\mu_{ab}/\rho)_0$ are the mass energy absorption coefficient for the N-th material and water, respectively, and $(\rho_{el})_N$ is the relative mass electron density of the N-th material (in electrons per unit mass) with respect to water.

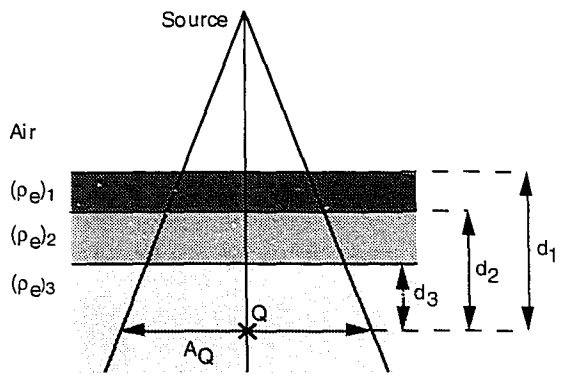

FIG. 6.2. *Schematic diagram of the parameters used for inhomogeneity correction using the generalized Batho power law. The diagram illustrates a phantom composed of three layers with relative electron densities of* $(\rho_e)_1$, $(\rho_e)_2$, and $(\rho_e)_3$.

So in order to understand the application of Eq. (6.3), one can consider the situation of Fig. 6.2 for a phantom composed of three different layers. The inhomogeneity correction factor calculated according to Eq. (6.3) for point Q can be given by:

$$C_i = K_3 \cdot TAR(d_1, A_Q)^{(\rho_e)_1-(\rho_e)_0} \cdot TAR(d_2, A_Q)^{(\rho_e)_2-(\rho_e)_1} \cdot TAR(d_3, A_Q)^{(\rho_e)_3-(\rho_e)_2}, \quad (6.5)$$

where $(\rho_e)_0=(\rho_e)_{water}=1$ by definition.

The calculation algorithm of the generalized Batho power law as used in *CADPLAN* is based on the formalism of Eq. (6.3),[6] however, K_N is always given the value of 1. The calculation is performed on a pixel-by-pixel basis where contours for internal structures are not needed. The external body contour, on the other hand, has to be defined by the operator. Since TAR is only defined for depths of d_{max} and beyond, the generalized Batho power law uses the TAR value at d_{max} in the dose build-up region. *CADPLAN* also supports another correction algorithm under the name "modified Batho power law". The modified Batho power law is identical to the generalized form with the exception that the

depth argument in the TAR is defined with reference to the depth of d_{max} as opposed to the surface. Hence Eq. (6.3) becomes:

$$C_i = K_N \prod_{m=1}^{N} TAR(d_{\max} + d_m, A_Q)^{(\rho_e)_m - (\rho_e)_{m-1}}. \tag{6.6}$$

6.1.2 The equivalent TAR (ETAR) method

The tissue-air ratio (TAR) method[7] was introduced as a correction method for inhomogeneities based on the ratio of TAR for the case of a phantom with the inhomogeneity over the TAR for the case of a completely homogeneous phantom. The depth argument of the TAR is corrected for the equivalent depth in water, so for the example of Fig. 6.1 the correction factor C_i is given by:

$$C_i = \frac{TAR(d', A_Q)}{TAR(d_1, A_Q)}, \tag{6.7}$$

where d' is the equivalent depth in water which for Fig. 6.1 is given by $d' = (d_1 - d_2)(\rho_e)_1 + (d_2 - d_3)(\rho_e)_2 + d_3(\rho_e)_3$, and A_Q is the field size at the calculation point Q.

The correction factor as calculated in Eq. (6.7) takes into account the effect of the primary beam attenuation, however, it does not account for the change in the scatter component. Therefore, Sontag and Cunningham[8] developed the equivalent TAR (ETAR) method with the intention of introducing a correction algorithm that accounts for the primary beam as well as for the geometric factors that are responsible for the scattered dose contribution. The ETAR method was designed for use in a CT based planning system where not only the depth but also the field size arguments are scaled as follows:

$$C_i = \frac{TAR(d', A'_Q)}{TAR(d, A_Q)}, \tag{6.8}$$

where d is the actual depth in phantom of the calculation point Q, d' is the water equivalent depth, A_Q is the field size at point Q, and A'_Q is the scaled field size. The parameter d' is calculated by averaging the relative electron densities ρ_e

for all the pixels from the surface to the point Q along the direct ray line connecting the source to Q. Mathematically, d' is given by:

$$d' = d \cdot \frac{1}{N} \sum_{i=1}^{N} (\rho_e)_i \,, \tag{6.9}$$

where N is the number of pixels lying along the rayline, and $(\rho_e)_i$ is the relative electron density of each individual pixel. The scaled field size A'_Q is given by:

$$A'_Q = A_Q \cdot (\rho_e)' = A_Q \cdot \frac{\sum_i \sum_j \sum_k (\rho_e)_{ijk} W_{ijk}}{\sum_i \sum_j \sum_k W_{ijk}}, \tag{6.10}$$

where $(\rho_e)'$ is a weighted volume average of the relative electron density, $(\rho_e)_{ijk}$ is the relative electron density for pixel ijk, W_{ijk} is the weight factor for pixel ijk.

The weighting factors represent the significance of each volume element in contributing to the dose due to scattered radiation at the point of calculation. The weighting factors can be calculated using angular Compton scatter cross-sections (Klein-Nishina) and integrating the scatter contribution over the irradiated volume. Another approach, also suggested by Sontag and Cunningham,[8] is to reduce the three dimensional integration to a two dimensional integration. This is accomplished by combining all the density information of the CT slices into a single "equivalent" slice:

$$(\rho_e)'_{ij} = \frac{\sum_k (\rho_e)_k W_k}{\sum_k W_k}, \tag{6.11}$$

where W_k are overall weighting factors for the effect of each slice in producing scatter seen in the CT slice where the dose distribution is to be produced. Each pixel element in the "equivalent" plane has relative electron density $(\rho_e)'_{ij}$ which is the weighted average of all pixels in each slice with the same i,j coordinates.

The equivalent slice then reduces the three dimensional integration of Eq. (6.10) to a two dimensional integration done in the equivalent plane, as follows:

$$A'_Q = A_Q \cdot \frac{\sum_i \sum_j (\rho_e)'_{ij} \cdot W_{ij}(Z_{eff})}{\sum_i \sum_j W_{ij}(Z_{eff})}, \qquad (6.12)$$

where Z_{eff} is the effective distance from the equivalent slice to the slice where the dose distribution is being calculated.

6.2 Comparison of the inhomogeneity correction algorithms

The literature indicates many studies aimed at verifying the various inhomogeneity correction algorithms.[4,9-11] However, the difficulty in providing a general statement about the overall accuracy of such algorithms can be attributed to the effects of the type, shape, size, and number of the inhomogeneities, as well as the effects of beam parameters (e.g., energy, shape) and relative position of the calculation point on the accuracy of the dose predicted by the correction algorithm. Therefore, only a qualitative assessment is provided in this section.

Most inhomogeneity correction algorithms were originally developed to provide a better dose estimate for the lung and thorax area. A comparison of two inhomogeneity correction algorithms used by *CADPLAN* (Table 6.1) shows that the generalized Batho power law is mainly a one dimensional approach as compared to the ETAR method which uses information available in 3D. However, both methods were derived from the ratio of tissue-air ratio principle which was developed for the slab geometry configuration. Both methods take into account the effect of path length and primary beam attenuation. For the scatter dose contribution, the generalized Batho power law is only sensitive to the depth position along the primary ray, whereas the ETAR uses three dimensional density scaling of the geometric parameters: depth and field size. While ETAR can account for the lateral shape of the inhomogeneity, the generalized Batho power law assumes a slab configuration for the

inhomogeneities extending to the full lateral limits of the beam. Furthermore, the generalized Batho power law considers only inhomogeneities found in the region above the point of calculation. As for secondary charged particle fluence, neither the Batho power law nor the ETAR are capable of correcting for changes in electron transport. All of these factors will have significant implications on the accuracy of each correction algorithm.

TABLE 6.1. *Comparison of the theoretical abilities of the generalized Batho power law and ETAR in correcting for tissue inhomogeneities.*

Capabilities	Generalized Batho	ETAR
Type	1-D	3D
Position of inhomogeneity	Yes, if above the point of calculation	Yes
Shape of inhomogeneity	No	Yes
Primary contribution	Yes	Yes
Scatter contribution	Only along primary	Density scaling of depth and field size
Electron transport	No	No

6.3 CT numbers to electron density conversion

To correct for inhomogeneities a CT-based treatment planning system relies heavily on the information provided by the CT images. A CT image is a reconstructed two-dimensional matrix of pixels where each pixel is given a value known as a CT number in Hounsfield units (HU). Previous studies[12-16] indicate that one can relate the relative electron density ρ_e with the CT number. The determination of the CT number for a given material depends on the individual CT scanner used, the image reconstruction algorithm, the size of the field of view, the kV_p used, and the location of the material in the phantom (center vs. close to the edge).[15,16] *CADPLAN* uses a linear relationship with a discontinuity in converting the CT number of each pixel to a corresponding relative electron density ρ_e. The software is shipped with the following two equations for the CT number to ρ_e conversion:

$$\rho_e = 1.00000 + 0.00100 \times \text{CT number} \quad \text{for CT numbers} \leq 100, \quad (6.13)$$

$$\rho_e = 1.05200 + 0.00048 \times \text{CT number} \quad \text{for CT numbers} > 100, \quad (6.14)$$

where ρ_e is the electron density relative to water and CT numbers are given in HU.

Equations (6.13) and (6.14) are based on Compton scatter imaging studies performed by Battista and Bronskill.[13] The validity of the two equations for our Picker PQ-2000 CT-simulator were studied and the results are presented in this section.

The PQ-2000 CT scanner reconstructs images of size 256x256 pixels with CT numbers ranging from -1000 (air) to +3000 (high atomic number material). The x-ray tube is calibrated to operate at a peak voltage of 120 kV_p and 130 kV_p. The CT number is dependent on the linear attenuation coefficient of material according to the following relationship:

$$\text{CT number} = K \cdot \left(\frac{\mu_p - \mu_w}{\mu_w}\right), \quad (6.15)$$

where K is a magnification factor equal to 1000 in most modern CT scanners, μ_p is the linear attenuation coefficient of the material scanned at the given pixel, and μ_w is the linear attenuation coefficient of water.

The linear attenuation coefficient for diagnostic energies in the range from 30 to 100 keV can be expressed in terms of the electronic cross section of the photoelectric effect σ_τ^e, Compton effect σ_C^e, and coherent (Rayleigh) scattering σ_{coh}^e interactions as follows:[17]

$$\mu = \rho \frac{N_A Z}{A} \cdot (\sigma_{coh}^e(E,Z) + \sigma_\tau^e(E,Z) + \sigma_C^e(E)), \quad (6.16)$$

where E is the effective energy of the beam, ρ is the mass density of the material, N_A is Avogadro's number (6.022×10^{23} atoms per gram-atom), Z is the atomic number of the material, and A is the atomic mass. The product $(\rho N_A Z/A)$ is the electron density (electrons/unit volume) for the material.

For photon beams with high energies additional terms for pair production and nuclear interactions should be added to Eq. (6.16) according to the ICRU.[18] However, for the case of CT energies, Eq. (6.16) is sufficient. By combining Eqs. (6.15) and (6.16), Battista and Bronskill[13] were able to relate relative electron density ρ_e to the CT number as follows:

$$\rho_e = R \cdot (1.000 + 0.001 \cdot \text{CT number}), \tag{6.17}$$

where R is given by

$$R = \frac{(\sigma^e_{coh} + \sigma^e_\tau + \sigma^e_C)_{water}}{(\sigma^e_{coh} + \sigma^e_\tau + \sigma^e_C)_{material}}. \tag{6.18}$$

Studies[13] have shown that R can in practice be considered unity for water, lung, muscle, and air in the range from 60 to 80 keV of effective beam energy, while a great deviation from unity in the value of R was observed for bone. This can be explained by the dependence of the coherent and especially the photoelectric interactions on the atomic number. CT images are obtained at diagnostic x-ray energies where photoelectric interactions are dominant and are greatly affected by the effective atomic number of material. On the other hand, at megavoltage therapeutic energies the Compton interaction is dominant and is greatly dependent on the electron density. In the human body soft tissue (Z_{eff}=7.35), muscle (Z_{eff}=7.62), lung (Z_{eff}=7.66), water (Z_{eff}=7.51), air (Z_{eff}=7.78) all have effective atomic numbers that are very close to each other, while bone has an effective atomic number that is approximately twice that of soft tissue (Z_{eff}=13.84 for cortical bone). As a result, the relationship linking relative electron density to CT number is found to consist of two linear parts: one for the low Z material, and one for the higher Z material with a discontinuity in between. The values for the effective atomic numbers were calculated according to the following equation[1] and using the elemental composition of each tissue as provided by the ICRU:[19]

$$Z_{eff} = (\sum_{i=1}^{n} a_i Z_i^m)^{1/m}, \tag{6.19}$$

where a_i is the fractional number of electrons per gram belonging to material of atomic number Z_i. There have been many published values for the exponent m in the literature.[1,17,20] However, a study by Johns and Cunningham[1] has concluded that in the photoeffect region the best fit was reached for m values ranging from 3.4 to 3.8 with the most of the best fit values ranging around 3.5. Therefore an exponent of 3.5 was used for all Z_{eff} calculated in this work.

The process employed for characterizing the relationship between CT number and relative electron densities for our Picker PQ-2000 CT-simulator was a modified version of previous work found in the literature.[12,15,16] A cylindrical CT phantom with a diameter of 32 cm and a thickness of 6 cm (Radiation Measurements Inc., Middleton, WI, USA) was used for this experiment. The phantom was made of a water equivalent material and provided for 9 identical holes where cylindrical plugs (with an average diameter of 4.5 cm) can be placed. A custom made vial was constructed to hold liquid solutions and to fit into the holes of the cylindrical phantom. A total of 12 different solutions/materials were used in our experiment (Table 6.2). The materials were grouped into two groups: a low Z group which consisted of air, hexane, methanol, water, and four dextrose solutions and a high Z group which consisted of four calcium chloride ($CaCl_2$) solutions.

In Table 6.2, the concentrations quoted for dextrose and $CaCl_2$ solutions represent the number of grams of solute per 100 mL of water, i.e., the 60% $CaCl_2$ solution represents 60 grams of $CaCl_2$ in 100 mL of water.

The materials listed in Table 6.2 were scanned at the center of the CT phantom using a field of view of 48x48 cm^2, a kVp of 130, a current of 100 mA, and an exposure time of 4 seconds. A single transverse slice of 256x256 pixels and thickness of 1 cm was constructed. The CT numbers for each material were measured by averaging the CT numbers inside a circle with an area of 709 mm^2 located entirely inside the borders of the cylindrical vial containing the material. The results of this experiment are illustrated in Fig. 6.3.

TABLE 6.2. *A list of materials used for CT calibration and their properties.*

Material	Density (gm/cm^3)	Z_{eff}	ρ_e
Low Z Material:			
Air @ NTP*	0.001	7.78	0.001
Hexane (C_6H_{14})	0.66	5.46	0.690
Methanol (CH_3OH)	0.77	6.80	0.779
Water (H_2O)	1.00	7.51	1.000
20% dextrose ($C_6H_{12}O_6$)	1.07	7.43	1.063
30% dextrose ($C_6H_{12}O_6$)	1.09	7.40	1.080
40% dextrose ($C_6H_{12}O_6$)	1.12	7.38	1.107
50% dextrose ($C_6H_{12}O_6$)	1.14	7.36	1.125
High Z Material:			
8.6% $CaCl_2$	1.07	9.75	1.059
17.6% $CaCl_2$	1.13	11.05	1.109
27.2% $CaCl_2$	1.20	11.86	1.168
60% $CaCl_2$	1.37	13.78	1.306

* NTP is for normal temperature (20° C) and pressure (101.3 kPa). The fractional content of air by weight was taken as N(0.755), O(0.232), A(0.013).[1]

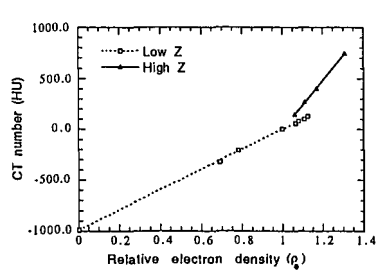

FIG. 6.3. *Relationship between CT numbers and relative electron densities for the Picker PQ-2000 CT-simulator.*

A linear fit to the data in Fig (6.3) shows that the relationships linking relative electron density ρ_e to CT numbers for our specific CT scanner can be given by the following two equations:

$$\rho_e = 1.00090 + 0.00101 \cdot \text{CT number} \qquad \text{for CT numbers} \leq 100, \qquad (6.20)$$

$$\rho_e = 1.00080 + 0.00041 \cdot \text{CT number} \qquad \text{for CT numbers} > 100. \qquad (6.21)$$

Equations (6.20) and (6.21) were implemented in *CADPLAN* for images collected using the Picker PQ-2000 CT-simulator. Moreover, further investigations into the effects of kV_p, size of the field of view, and location of the material (center of the phantom versus peripheral location) were studied. The change of the kV_p from 130 to 120 was found to have a negligible effect on low Z material where the variation of CT numbers was less than 2 HU; however, for high Z material the change was slightly more dramatic and could reach as much as 52 HU (6.7%) for the 60% $CaCl_2$ solution. Changing the field of view from 48x48 cm^2 to 24x24 cm^2 was also found to have an insignificant effect on the CT numbers for low Z material; however, the high Z solutions were affected by as much as 78 HU (9.9%). Displacing the scanned material radially from the center of the CT phantom by a distance of 12 cm was found to have no effect on the CT numbers produced for the low Z material, and very little effect (26 HU or less than 3.5% change for the 60% $CaCl_2$ solution) on the CT numbers for high Z material.

To put these results into perspective one has to consider the impact of the uncertainty in CT number determination on the calculation of relative electron density. Changes in the kV_p, size of field of view, and relative position of the material were found to have no effect on CT numbers for low Z material. However, for high Z material the maximal variation observed was 78 HU or 9.9%. Such an uncertainty in the determination of CT numbers for high Z material would correspond to a maximal uncertainty of 0.03 (2.5%) in the determination of relative electron density for our CT scanner according to Eq. (6.21). Such a variation has no significant effects on the calculation of the inhomogeneity correction factor.[16,21,22] Therefore Eqs. (6.20) and (6.21) can be considered representative of our scanner, however, great care should be taken for points found in the discontinuity region.

6.4 Testing configurations

The testing configurations used in our experiments were composed of three stages designed in ascending order of complexity: (1) single beam - single inhomogeneity, (2) single beam - multiple inhomogeneities, and (3) an overall configuration simulating a clinical case. Thermoluminescent dosimeters were used to measure the dose distribution for all inhomogeneity cases. For each case the measured data were compared with calculated dose distributions using the generalized Batho power law, the modified Batho power law, and the Equivalent TAR method.

6.4.1 Single beam - single inhomogeneity

A single flat slab of inhomogeneity was inserted into a homogeneous phantom of white polystyrene (density = 1044 kg/m^3, ρ_e= 1.011). The polystyrene phantom consisted of 3.2 mm thick square flat slabs with an area of 30x30 cm^2. The inhomogeneity slab was inserted at a depth of 5 cm in the polystyrene phantom. Two different inhomogeneity materials were used: lung equivalent and hard bone equivalent material (Radiation Measurement Inc., Middleton, WI, USA). They both represent the two extremes of tissue inhomogeneities that are encountered clinically. The lung equivalent material had a density of 310 kg/m^3 and relative electron density of 0.299, while the hard bone equivalent material had a density of 1840 kg/m^3 and a relative electron density of 1.710.[19,23] The two materials were developed according to an epoxy resin formula developed by White et. al. in 1977.[23] A thickness of 8 cm was used for the lung equivalent material and 3 cm for the bone equivalent material.

A 10x10 cm^2 square open beam was used to irradiate the phantom orthogonally to the surface. The central axis PDD was measured using TLD rods for two photon energies: cobalt-60 and 10 MV and for two single inhomogeneities: lung and bone. The measurement points consisted of points above the inhomogeneity, within the inhomogeneity, at the boundary of the inhomogeneity, and beyond the inhomogeneity, thereby covering a depth range from d_{max} to 21 cm for lung and d_{max} to 16 cm for bone.

Figure 6.4 illustrates the percentage depth doses gathered from these experiments. The results demonstrate the effect of the type of the

inhomogeneity on the accuracy of the correction algorithm. While the correction algorithms used by *CADPLAN* were able to handle the lung case rather satisfactorily as expected, the case of bone provided relatively large discrepencies between measurement and calculation, especially at the boundary and within the inhomogeneity where changes in electron transport are dominant. A quantitative comparison of calculated versus measured dose confirms this statement. Table 6.3 lists the root-mean-square error for each of the three correction algorithms. The error was calculated in a similar manner to that used in the previous chapters according to Eq. (5.1). Furthermore, Table 6.3 makes it evident, as one would expect, that the application of an inhomogeneity correction method is likely to produce a more accurate dose distribution than that produced without an inhomogeneity correction for the slab geometry.

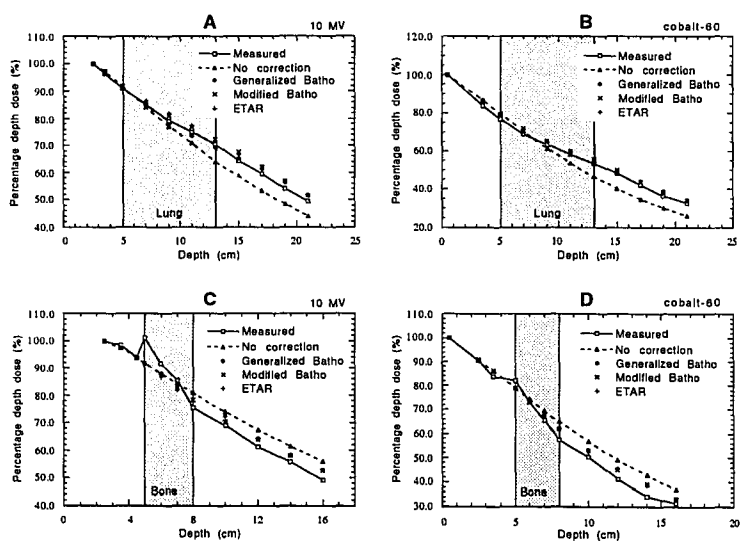

FIG. 6.4. *Central axis percentage depth dose results in an inhomogeneous phantom in the slab geometry. Parts* ***A*** *and* ***B*** *are the results found for lung as an inhomogeneity for the 10 MV beam and the cobalt-60 beam, respectively. Parts* ***C*** *and* ***D*** *illustrate the results for bone as an inhomogeneity for the 10 MV beam and the cobalt-60 beam, respectively.*

TABLE 6.3. *A list of the root-mean-square error calculated by comparing the measured central axis percentage depth dose to that produced by each of the three inhomogeneity correction algorithms.*

	Lung		Bone	
Correction Algorithm	10 MV	cobalt-60	10 MV	cobalt-60
No correction	7.0	12.1	7.4	12.7
Generalized Batho	2.3	3.5	5.1	6.7
Modified Batho	3.2	3.7	4.5	6.5
ETAR	3.1	3.5	4.7	6.1

6.4.2 Single beam - multiple inhomogeneities

For this configuration an anthropomorphic phantom was used. The Alderson Rando Phantom (Alderson Research Laboratories Inc., Stamford, CT, USA) is a solid anthropomorphic phantom representing the head, thorax, and pelvic portions of an adult North American male of 175 cm height and 73.5 kg mass.[24] The phantom is composed of an isocyanate rubber-based muscle substitute, an epoxy resin-based lung substitute, and an embedded natural human skeleton. The phantom is cut into 34 transverse sections of 2.5 cm thickness. Each slab houses a 2D matrix of small cylindrical holes. The holes are separated by 3 cm and are filled with plugs for the placement of TLD dosimeters. The thorax region of the anthropomorphic phantom was first scanned in the supine position using the Picker PQ-2000 CT-simulator (Picker International, Highland Heights, OH, USA) and the CT images were transferred to *CADPLAN*. A single anterior-posterior open beam of 10x10 cm^2 at the nominal SSD was used to irradiate the right lung with the central axis impinging on transverse section #15 of the Rando phantom. A total of 21 comparison points covering areas in lung, bone, and muscle were measured using TLDs in the central axis plane (Fig. 6.5). The measured data were compared with the three correction algorithms of *CADPLAN* for both cobalt-60 and 10 MV beams.

FIG. 6.5. (shown on the next page) *A schematic illustration of the test geometry for the thorax region of the anthropomorphic phantom. The transverse slice was taken at the center of the incident beam. The black dots represent the location where special plugs were loaded with TLD rods in order to measure the relative dose within the irradiated volume.*

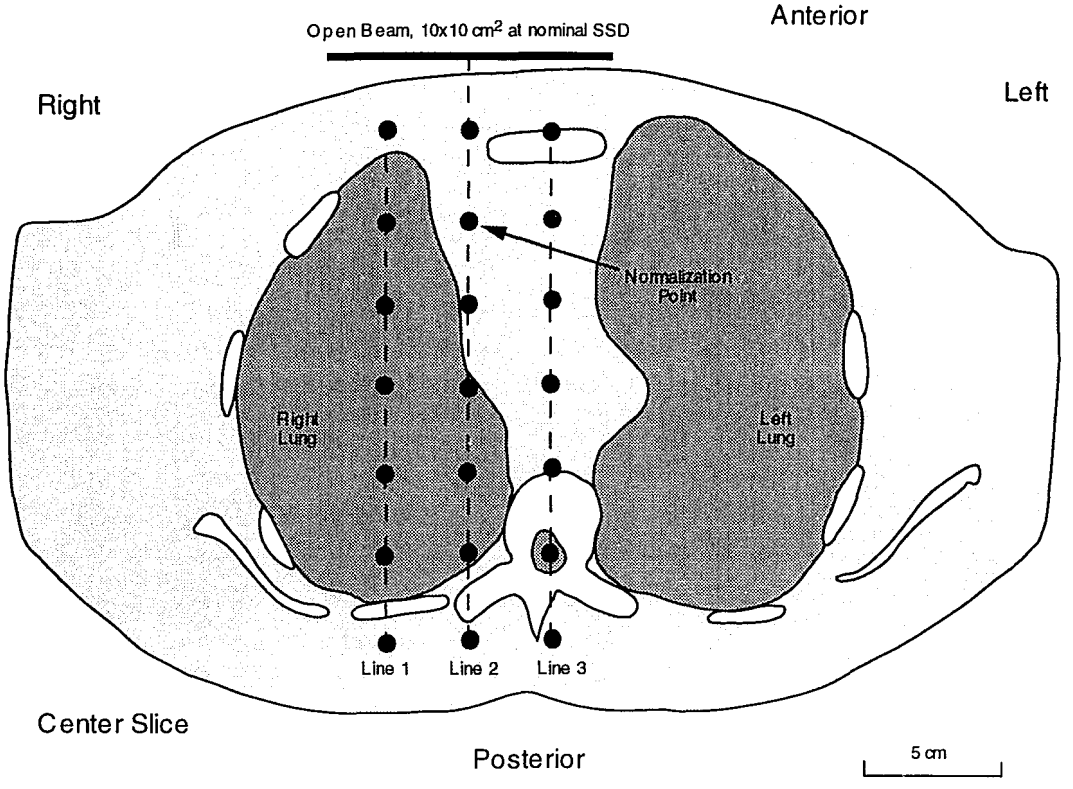
Open Beam, 10x10 cm2 at nominal SSD
Anterior
Right
Left
Normalization Point
Right Lung
Left Lung
Line 1
Line 2
Line 3
Center Slice
Posterior
5 cm

This configuration represents an extreme situation where lung is found in a large part of the irradiated volume. It is also very different from the slab configuration of Section 6.4.1, in that the relative electron density varies laterally across the beam. This results in a fundamental change of the pattern of scattered photons in addition to the change in electron transport inside and along the lateral borders of the inhomogeneities. Therefore this experiment will test the combination of the inherent inaccuracy of the inhomogeneity correction method and the inaccuracy of its implementation within *CADPLAN*.

In order to consider the various effects for the case of Fig. 6.5, one can simplify the two dimensional matrix of comparison points into three one dimensional lines. Line 1 consists of a number of points that are positioned well inside the lung inhomogeneity, while line 2 comprises a number of points close to the lung-muscle interface where changes in electron transport are responsible for dose modification. On the other hand, the primary beam along line 3 passes through part of the sternum and mostly through muscle material. The dose to points along line 3 are affected by primary beam attenuation as well as the reduced lateral photon scatter from both lungs.

The relative dose measured using TLDs was normalized to the point at a depth of 5.3 cm along the central axis as indicated in Fig. 6.5. The relative dose values of measured points along the three lines 1,2, and 3 (Fig. 6.5) were compared to relative dose values calculated by *CADPLAN* for the 10 MV (Fig. 6.6) and the cobalt-60 beams (Fig. 6.7).

Figures 6.6 and 6.7 show the tendency for the inhomogeneity correction algorithms to overcorrect and overestimate the dose to the points within the lung (line 1). As expected, none of the inhomogeneity correction algorithms were able to account for changes in electron transport (line 2). Furthermore, none of the correction algorithms were able to account for the reduction in lateral scatter (line 3). The root-mean-square errors calculated using the entire set of comparison points are listed in Table 6.4 for each individual correction algorithm.

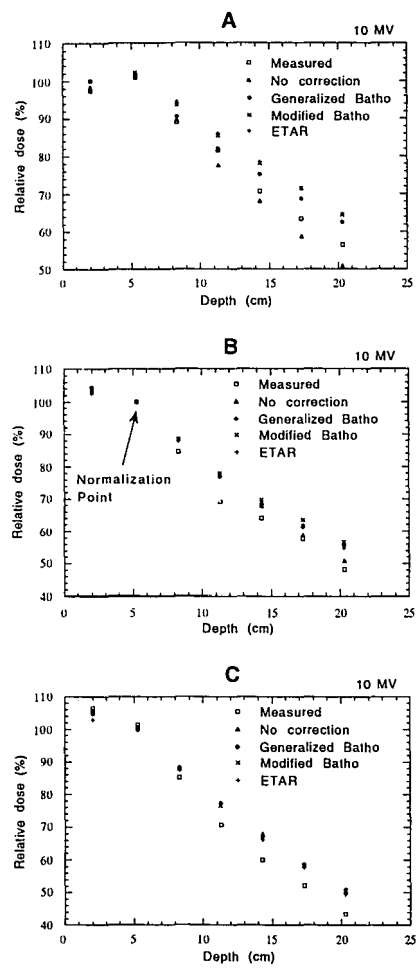

FIG. 6.6. *A comparison of measured relative dose values versus calculated values using a 10 MV beam incident on the thorax region of the anthropomorphic phantom. Part* ***A***, ***B***, *and* ***C*** *represent the data points along line 1, 2, and 3, respectively.*

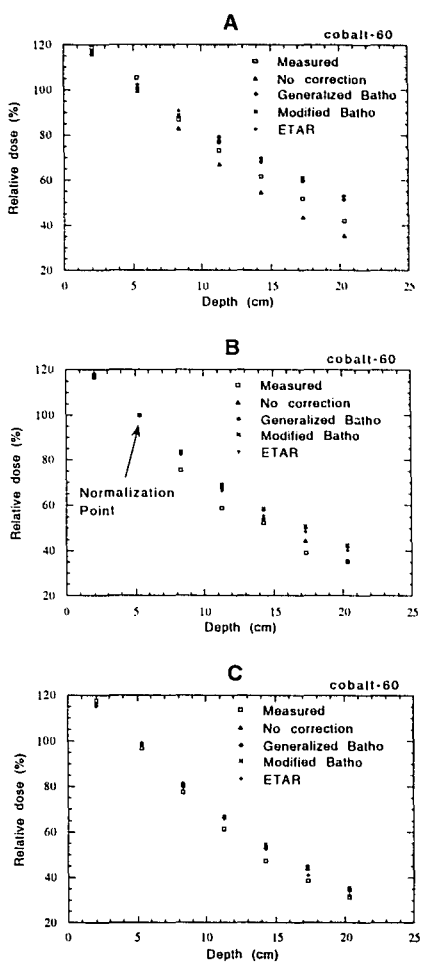

FIG. 6.7. *A comparison of measured relative dose values versus calculated values using a cobalt-60 beam incident on the thorax region of the anthropomorphic phantom. Part* ***A, B,*** *and* ***C*** *represent the data points along line 1, 2, and 3, respectively.*

TABLE 6.4. *A list of the root-mean-square error calculated by comparing the relative dose distribution measured at the points indicated in Fig. 6.5 to the data calculated by each of the three inhomogeneity correction algorithms.*

	Thorax	
Correction Algorithm	10 MV	cobalt-60
No correction	7.2	9.5
Generalized Batho	8.2	12.7
Modified Batho	9.3	13.6
ETAR	8.5	11.3

6.3.3 Clinical geometry

This configuration is aimed at providing an overall testing configuration to the treatment planning system which involves multiple beams, contour correction, and a realistic inhomogeneity correction. The anthropomorphic phantom was used to simulate the treatment for a prostate carcinoma using the four beam box technique. The pelvic region of the anthropomorphic phantom was scanned in the supine position using our Picker PQ-2000 CT-simulator and the CT images were transferred to *CADPLAN* for planning. Since cobalt-60 is not an appropriate energy for treatment of prostate, the verification was only carried out with the 10 MV beams in order to simulate a realistic treatment configuration. Four *isocentric* coplanar open fields were arranged in the standard box format in a manner appropriate to the phantom's anatomy with the central plane occurring at transverse section #32 of the Rando phantom (see Fig. 6.8). Table 6.5 lists the parameters pertaining to each individual field.

FIG. 6.8. (shown on the next page) *A schematic illustration of the test geometry simulating the prostate case using the anthropomorphic phantom. The transverse slice was taken at the center of the incident beams, i.e., isocenter level. The black dots represent the location where special plugs were loaded with TLD rods in order to measure the relative dose within the irradiated volume.*

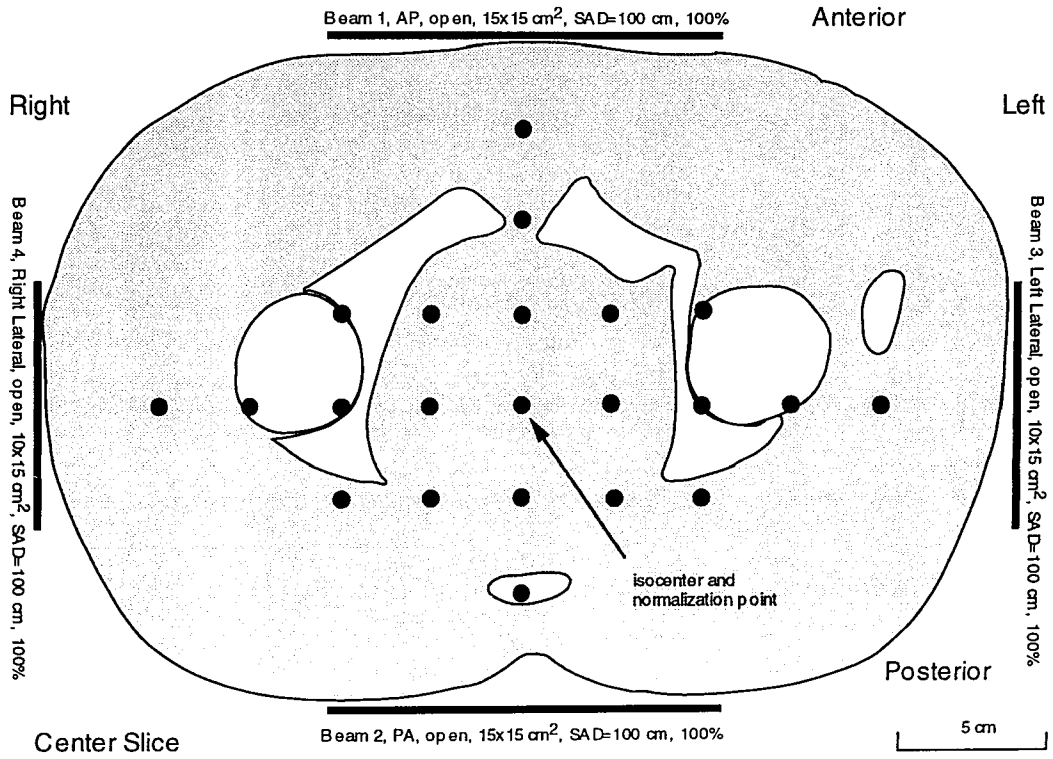
Beam 1, AP, open, 15x15 cm2, SAD=100 cm, 100%
Anterior
Right
Left
Beam 4, Right Lateral, open, 10x15 cm2, SAD=100 cm, 100%
Beam 3, Left Lateral, open, 10x15 cm2, SAD=100 cm, 100%
isocenter and
normalization point
Posterior
Center Slice
Beam 2, PA, open, 15x15 cm2, SAD=100 cm, 100%
5 cm

TABLE 6.5. *A list of the beam parameters for the prostate treatment simulation.*

Beam #	Beam Name	Field Size (cm^2)	Gantry Angle	Collimator Angle	Wedge	Weight	SSD (cm)
1	AP*	15x15	0°	0°	0	100%	88.0
2	PA*	15x15	180°	0°	0	100%	91.9
3	left lateral	10x15	90°	0°	0	100%	84.1
4	right lateral	10x15	270°	0°	0	100%	84.4

* AP = anterior-posterior, PA = posterior-anterior

The results of this experiment are illustrated in Fig. 6.9. Given the uncertainty of positioning and the uncertainty in TLD dosimetry, the measured dose values show a satisfactory agreement with the calculated dose distribution. The points responsible for the large percentage error (of the order of 10%) shown in the histograms of Fig. 6.9 originated from points taken within and around the bone-structure of the pelvic area (Fig. 6.8). The application of inhomogeneity correction provided a slight improvement to the dose distribution. However, a big improvement is not expected since significant differences due to inhomogeneity corrections occur mainly for lung tumors and less dramatically for a prostate case involving bone inhomogeneities.[25] Differences among the three correction algorithms were not significant in this study.

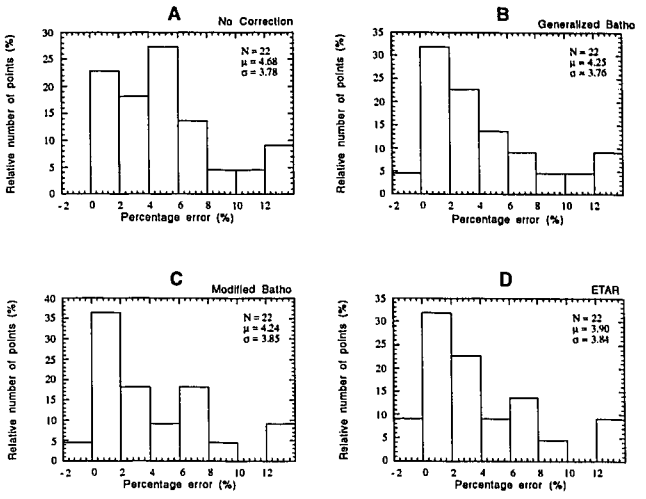

FIG. 6.9. *The error histogram for the clinical case simulating prostate treatment. Each histogram includes all the comparison points for each correction algorithm. Parts* ***A, B, C,*** *and* ***D*** *display the percentage error histogram for the case of no correction, generalized Batho power law correction, modified Batho power law correction, and ETAR correction, respectively. The total number of points N, mean value* μ *of the error, and standard deviation* σ *of the error are also indicated for each histogram.*

6.5 Summary

In this chapter an overview of the inhomogeneity correction algorithms of *CADPLAN* was presented and a detailed dosimetric verification was carried out. However, prior to the verification, a calibration of the relative electron density versus CT numbers for our CT-simulator was carried out and the results were given. The test cases covered single inhomogeneities in a slab geometry, the use of the anthropomorphic phantom to evaluate the dose distribution in the lung, as well as a simulated clinical case involving prostate treatment. There was no significant difference observed in the dose distribution produced by *CADPLAN*, whether the generalized Batho power law, the modified Batho

power law, or the ETAR method was used. The inhomogeneity correction algorithms produced excellent results for lung equivalent material placed in a slab geometry. However, for the thorax case, the correction algorithms had the tendency to overestimate the dose for points within the lung, which is in agreement with published results of a similar study.[26] Furthermore, the correction algorithms were unable to properly account for scattered photons especially in the case where the type of inhomogeneity material varied laterally across the beam. As expected, no inhomogeneity correction algorithm available commercially including *CADPLAN's* (with the exception of Monte Carlo simulation methods) can fully account for variations in electron transport.[27]

6.6 References

1 H. E. Johns and J. R. Cunningham, *The Physics of Radiology*, 4th ed. (Charles Thomas, Springfield, IL, 1983).

2 H. F. Batho, "Lung corrections in Co-60 beam therapy," J. Can. Assoc. Radiol. **15**, 79-83 (1964).

3 M. R. Sontag and J. R. Cunningham, "Corrections to absorbed dose calculations for tissue inhomogeneities," Med. Phys. **4**, 431-436 (1977).

4 S. Webb and R. A. Fox, "Verification by Monte Carlo methods of a power law tissue-air ratio algorithm for inhomogeneity corrections in photon beam dose calculations," Phys. Med. Biol. **25**, 225-240 (1980).

5 K. J. Cassell, P. A. Hobday, and R. P. Parker, "The implementation of a generalised Batho inhomogeneity correction for radiotherapy planning with direct use of CT numbers," Phys. Med. Biol. **26**, 825-833 (1981).

6 Varian Oncology Systems, *External beam modeling reference manual CADPLAN 2.62*, ver. 1.1, (Varian-Dosetek Oy, Espoo, Finland, 1995).

7 International Commission on Radiation Units and Measurements, ICRU Report No. 24. "Determination of absorbed dose in a patient irradiated by beams of X or gamma rays in radiotherapy procedures" (ICRU, Washington, D.C., 1976).

8 M. R. Sontag and J. R. Cunningham, "The equivalent tissue-air ratio method for making absorbed dose calculations in a heterogeneous medium," Radiology **129**, 787-794 (1978).

9 M. E. Young and J. D. Gaylord, "Experimental tests of corrections for tissue inhomogeneities in radiotherapy," Br. J. Radiol. **43**, 349-355 (1970).

[10] W. L. Tang, F. M. Khan, and B. J. Gerbi, "Validity of lung correction algorithms," Med. Phys. **13**, 683-686 (1986).

[11] C. Kappas and J. C. Rosenwald, "Quality control of inhomogeneity correction algorithms used in treatment planning systems," Int. J. Radiat. Oncol. Biol. Phys. **32**, 847-858 (1995).

[12] R. P. Parker, P. A. Hobday, and K. J. Cassell, "The direct use of CT numbers in radiotherapy dosage calculations for inhomogeneous media," Phys. Med. Biol. **24**, 802-809 (1979).

[13] J. J. Battista and M. J. Bronskill, "Compton scatter imaging of transverse sections: an overall appraisal and evaluation for radiotherapy planning," Phys. Med. Biol. **26**, 81-99 (1981).

[14] International Commission on Radiation Units and Measurements, ICRU Report No. 42. "Use of computers in external beam radiotherapy procedures with high-energy photons and electrons" (ICRU, Washington, D.C., 1987).

[15] E. C. McCullough and T. W. Holmes, "Acceptance testing computerized radiation therapy treatment planning systems: Direct utilization of CT scan data," Med. Phys. 12, 237-242 (1985).

[16] C. Constantinou, J. C. Harrington, and L. A. DeWerd, "An electron density calibration phantom for CT based treatment planning computers," Med. Phys. 19, 325-327 (1992).

[17] E. C. McCullough, "Photon attenuation in computed tomography," Med. Phys. **2**, 307-320 (1975).

[18] International Commission on Radiation Units and Measurements, ICRU Report No. 33. "Radiation quantities and units" (ICRU, Washington, D.C., 1980).

[19] International Commission on Radiation Units and Measurements, ICRU Report No. 44. "Tissue substitutes in radiation dosimetry and measurement" (ICRU, Washington, D.C., 1989).

[20] D. R. White, "An analysis of the Z-dependence of photon and electron interactions," Phys. Med. Biol. **22**, 219-228 (1977).

[21] R. A. Geise and E. C. McCullough, "The use of CT scanners in megavoltage photon-beam therapy planning," Radiology **124**, 133 (1977).

[22] S. C. Prasad, G. P. Glasgow, and J. A. Purdy, "Dosimetric evaluation of a computed tomography system," Radiology **130**, 777-781 (1979).

[23] D. R. White, R. J. Martin, and R. Darlison, "Epoxy resin based tissue substitutes," Br. J. Radiol. **50**, 814-821 (1977).

[24] International Commission on Radiation Units and Measurements, ICRU Report No. 48. "Phantoms and computational models in therapy, diagnosis and protection" (ICRU, Washington, D.C., 1992).

[25] Photon Treatment Planning Collaborative Working Group, "Role of inhomogeneity corrections in three-dimensional photon treatment planning," Int. J. Radiat. Oncol. Biol. Phys. **21**, 59-69 (1991).

[26] M. E. Masterson, G. Barest, C. Chen-Shou, K. Dopke, R. D. Epperson, W. B. Harms, K. E. Krippner, R. Mohan, E. D. Slessinger, M. R. Sontag, M. M. Urie, R. E. Wallace, and J. W. Wong, "Interinstitutional experience in verification of external photon dose calculations," Int. J. Radiat. Oncol. Biol. Phys. **21**, 37-58 (1991).

[27] J. W. Wong and J. A. Purdy, "Review of methods of inhomogeneity corrections," in Advances in Radiation Oncology Physics: Dosimetry, Treatment Planning, and Brachytherapy, edited by J. A. Purdy, AAPM monograph 19, 886-899, (American Institute of Physics, New York, 1992).

Chapter 7:
Performance Evaluation and Quality Assurance of the Treatment Planning System

7.1 Overall performance rating

The *CADPLAN* treatment planning system underwent a comprehensive dosimetric exam during this work. Our testing program covered configurations that were relevant to two treatment units: the Theratron-780 cobalt-60 beam and the Clinac-18 10 MV beam. The testing geometries ranged in difficulty from standard water phantoms to complex configurations simulating a clinical situation. The testing methodology illustrated the need for more accurate and convenient dosimetry methods. A treatment planning system is used for the purpose of predicting the behavior of the treatment unit and under most clinical situations this is true. However, there are incidences where the treatment unit acts differently from the presumed way, as demonstrated in the case of photon arc therapy, and the cause of the discrepancy then should be evaluated. The overall performance of *CADPLAN* can be evaluated from two aspects: *dosimetric* performance and *non-dosimetric* performance.

7.1.1 Dosimetric evaluation

Dosimetric performance covers all aspects relating to dose calculation accuracy, which was the primary aim of this work. *CADPLAN* was found to be in excellent agreement with measured dose distributions for the standard and complex geometry cases discussed earlier (Chapter 5). As for inhomogeneity

corrections, the performance of *CADPLAN* was representative of the accuracy of the correction algorithms. The corrections were most accurate for the slab geometry involving lung as an inhomogeneity. For the examination of each individual dosimetric configuration, the reader should refer to the corresponding section in the previous chapters. There is always a natural bias to point out the imperfections during an evaluation process and the following is a number of remarks concerning some observed shortcomings of the dosimetric aspect in the treatment planning system:

- *Tangential fields:* a serious logical error was discovered for tangential fields where the beam's central axis does not intersect the contour of the patient (see Section 5.2.2). This problem has a number of repercussions for current and future treatment techniques used in our clinic.

- *Inhomogeneity correction:* the inhomogeneity correction algorithms available in *CADPLAN* might be the most accurate methods available commercially at this time, however, our study indicated that a better accuracy is necessary for treatment cases where inhomogeneity correction is most critical, i.e., the thorax and lungs.

- *Dose calculation area:* the dose calculation area is always smaller than the area defined by the contour of the patient even when the patient's contour is much smaller than the maximal calculation area. Furthermore, the calculation area is always centered at the center of the CT image, and the maximal calculation dimensions do not cover the entire CT slice. This means that for some cases the CT slice needs to be shifted in order to place the region of interest within the calculation grid. The part of the CT slice that was pushed outside the display after a shift is not recoverable.

- *Isocentric normalization:* there is a limited freedom in plan normalization of SAD fields, despite three default options provided by *CADPLAN*. This might be an inconvenience to certain clinics, such as ours, that have developed their own suitable normalization procedure which happens to be different from *CADPLAN's* standard options. The only way around this obstacle is for the operator to renormalize each individual isocentric plan, thereby

introducing another potential source of error to the treatment planning process.

7.1.2 Non-dosimetric evaluation

The non-dosimetric evaluation covers all other aspects of the treatment planning system that are not primarily involved in dosimetry. This includes capabilities, such as CT image manipulation, 3D functions, user interface, etc. Even though the dosimetric aspect of *CADPLAN* was the main scope of this project, the constant interaction with the treatment planning system as a whole warrants a summary of the overall system's performance.

Overall, *CADPLAN* provides a number of useful tools for the facilitation of the treatment planning process. Its 3D abilities, which include non-coplanar planning, beam's eye view, CT slice reconstruction, digitally reconstructed radiographs, and volume histograms, are very robust. The user interface is based on nested menus that would generally allow the option for either keyboard or mouse inputs. The following is a number of remarks concerning the non-dosimetric aspects that could be improved in the *CADPLAN* treatment planning system:

- *Dose profile:* *CADPLAN* allows the user to calculate the dose profile along any arbitrary line. This line, however, can only be defined by a mouse. The ability to define the line by typing the coordinates by keyboard not only would improve accuracy, especially during commissioning, it would also speed up the verification process.

- *Image window and level:* it is impossible to change the image level and window during planning of a patient. *CADPLAN* does allow for image level and window manipulation only outside of the planning environment and once the patient is loaded into the planning program the image window and level revert to the default settings according to the system configuration.

- *CT numbers:* CT numbers in *CADPLAN* are not in Hounsfield units (HU). A *CADPLAN* CT number is equivalent to HU+1000,i.e., air has a CT number of 0 while water has a CT number of 1000 within *CADPLAN*. Most likely the

internal algorithm of *CADPLAN* needed to avoid negative CT numbers, however, such CT number representation could have been kept internal in the calculation code without the need for user notification. Such diversion from the conventional norm might be a cause for confusion.

- *CT numbers vs. relative electron densities:* the calibration of CT numbers versus relative electron densities can only be done using a single CT slice containing the entire set of calibration material. One cannot enter the calibration curve as a set of points nor as set of equations.

- *The overall user interface* is functional and practical. Nevertheless, with the exception of very well trained operators, the user can easily become disoriented among the different menus and submenus. This is because of the great similarity in appearance among all the nested command menus available.

7.2 Quality assurance in treatment planning

After the initial acceptance testing and verification a regular quality assurance (QA) program is necessary to insure a certain standard of reproducibility throughout the operation. Quality assurance of a modern 3D treatment planning system is complex and involves a great deal of care in implementing. A modern system treatment planning system may be the result of many tens of person-years of work producing as much as a million lines of code.[1] It is reasonable to expect a number of errors to remain in the program even for a well designed and well tested treatment planning system.[2] Throughout clinical use, each aspect of the treatment planning system might be subjected to a very large number of configurations, making it impossible to carry out an exhaustive test covering all permutations for one aspect of the treatment planning system, let alone for the entire system. Nevertheless, a QA program is essential to ensure proper practice.

The quality assurance program could take on many different formats which could include chart checks, database backup, and equipment maintenance. However, any QA program should consist of three fundamental parts: *software verification*, *dosimetric verification*, and *non-dosimetric*

verification. The *software verification test* is designed to ensure the constancy of all the treatment planning program files as well as all the data files for the various treatment units. Such a test could be carried out automatically using software diagnostic programs to detect any variation in the binary sequence of such files. Such test software could be provided by the manufacturer and may require additional training on the part of the operator. Another check should be aimed at verifying the stability of the data storage medium (the medium where the treatment planning program and all relevant files are stored). Any discrepancy should be investigated and corrected according to the situation.

The *dosimetric verification* part of the QA program is most important and critical. The extent of the QA tests implemented will depend on the treatment planning system in question as well as on the complexity of treatment techniques implemented in the clinic. Such QA programs are often subject to a cost-benefit consideration, however, a minimum acceptable standard should be observed. The tests outlined in this work (Table 3.3) are suitable for the initial acceptance and commissioning of a treatment planning system. By implementing an acceptance test such as ours, the clinical physicists would build a dosimetry library of comparison points for each individual test configuration. Carrying out such an extensive testing protocol in a regular QA program might be very time consuming, nevertheless, our testing protocol could still be modified so as to become suitable for regular checks. The major modification might be the reduction of the number of comparison points in each individual configuration. The various different testing configurations should be adhered to and not reduced. In fact new testing configurations might be added as new tools and new treatment techniques are introduced, such as a multileaf collimatór, a dynamic wedge, etc. In addition to this work, the literature lists a number of studies that could be used as guidelines in implementing a dosimetric QA program.[3,4] Because of the relative stability of computers, given the current high technology standards, the frequency of such tests should have a minimum of two times annually. In addition, the test frequency needs to be increased after every modification of the treatment planning system, e.g., software update and beam data modification.

Non-dosimetric verification, as the name implies, is aimed at verifying all the other aspects of the treatment planning system. For CT based 3D treatment

planning systems, the non-dosimetric verification is concerned mainly with the inspection of the 3D image information and its manipulation. Three dimensional image examination is a two fold task. The first is the investigation of the proper operation of the CT scanner in acquiring 3D images; the second is the investigation of the proper 3D reconstruction and manipulation of CT imager data in the treatment planning system. The evaluation and quality assurance of CT scanner operation and 3D display systems are beyond the scope of this study, but the literature points to a number of studies and recommendations.[5-8] Fraass et. al.[1] provide a very informative list of functions that should be considered when evaluating the non-dosimetric aspect of a treatment planning system.

In addition to the program outlined in Table 3.3, routine chart checks should remain an essential part of dosimetric regular checks. Chart checks are aimed at carrying out a brief manual check to patient input information, beam parameters, points of interest, relative dose distribution, absolute dose settings (treatment time or monitor units), and an overall consistency appraisal of the treatment planning process. Ideally, in vivo dosimetry is used as a final check to the planning procedure. However, in vivo dosimetry is only available at large centers, and even then, because of practical reasons, is only used for new or highly specialized treatment procedures.

7.3 Future work

It is evident that acceptance testing and quality assurance for treatment planning systems is an essential requirement for contemporary radiotherapy and should be part of the routine responsibilities of the clinical/medical physicists. Such verification will serve as a preventative protocol for potential errors and as a good opportunity to discover the abilities and limitations of the particular treatment planing system.

Future treatment planning is expected to be most influenced by two aspects: dose distribution modeling and treatment plan optimization. On the one hand, Monte Carlo methods for dose distribution calculations are believed to be the most accurate since they are based on first principles of radiation physics. Current computer hardware and programming techniques impose

practical limitations on using Monte Carlo methods for daily treatment planning. Such complex techniques might not be necessary for standard cases, however, for complex cases (such as a complicated inhomogeneity geometry, or a high Z inhomogeneity) Monte Carlo methods might provide an excellent clinical tool. On the other hand, current improvements of the field of radiotherapy are aiming at an improved level of dose optimization using spatial intensity modulation, which is placing additional demands on treatment planning systems of the future. Automatic 3D optimization of treatment plans will most likely become an essential requirement for any treatment planning system. This will complicate the design of acceptance testing and quality assurance procedures making such tests responsible for verifying the optimization algorithm in addition to the final dose distribution. In order for the dosimetric verification system to be practical and reasonable in time consumption, a practical 3D based dosimetry method is a necessity. Three dimensional dose plotters, film, and TLDs can be used to collect a complete three dimensional dose distribution, however, a great compromise in the calculation grid is needed to render such methods practical.

7.4 References

1 B. A. Fraass, D. L. McShan, and M. K. Martel, "Quality assurance for 3D treatment planning," in *3D Radiation Treatment Planning and Conformal Therapy*, edited by J. A. Purdy and B. Emami, 75-93 (Medical Physics, Madison, WI, 1993).

2 J. Jacky and C. P. White, "Testing a 3D radiation therapy planning program," Int. J. Radiat. Oncol. Biol. Phys. **18**, 253-261 (1990).

3 J. Van Dyk, R. B. Barnett, J. E. Cygler, and P. C. Shragge, "Commissioning and quality assurance of treatment planning computers," Int. J. Radiat. Oncol. Biol. Phys. **26**, 261-273 (1993).

4 American Association of Physicists in Medicine Task Group 23, AAPM Report No. 55. "Radiation treatment planning dosimetry verification," (American Institute of Physics, New York, 1995).

5 American Association of Physicists in Medicine Task Group 53, "Quality assurance of radiotherapy treatment planning systems," work in progress.

6 American Association of Physicists in Medicine, AAPM Report No. 1. "Phantom for performance evaluation and quality assurance of CT scanners," (American Institute of Physics, New York, 1977).

[7] American Association of Physicists in Medicine Task Group 2, AAPM Report No. 39. "Specification and acceptance testing of computed tomography scanners," (American Institute of Physics, New York, 1993).

[8] E. C. McCullough, "Specifying and evaluating the performance of computed tomography (CT) scanners," Med. Phys. **7**, 291-296 (1980).

List of Figures

List of Tables

Bibliography

- American Association of Physicists in Medicine, AAPM Report No. 1. "Phantom for performance evaluation and quality assurance of CT scanners," (American Institute of Physics, New York, 1977)..... 125

- American Association of Physicists in Medicine Task Group 2, AAPM Report No. 39. "Specification and acceptance testing of computed tomography scanners," (American Institute of Physics, New York, 1993)..... 125

- American Association of Physicists in Medicine Task Group 40, AAPM Report No. 46. "Comprehensive QA for radiation oncology" (American Institute of Physics, New York, 1994)..... 7

- American Association of Physicists in Medicine Task Group 45, AAPM Report No. 47. "AAPM code of practice for radiotherapy accelerators" (American Institute of Physics, New York, 1994)..... 7

- American Association of Physicists in Medicine Task Group 23, AAPM Report No. 55. "Radiation treatment planning dosimetry verification", (American Institute of Physics, New York, 1995)..... 51, 67, 71, 124

- American Association of Physicists in Medicine Task Group 53, "Quality assurance of radiotherapy treatment planning systems," work in progress.. 125

- H. F. Batho, "Lung corrections in Co-60 beam therapy," J. Can. Assoc. Radiol. **15**, 79-83 (1964)..... 94

- J. J. Battista and M. J. Bronskill, "Compton scatter imaging of transverse sections: an overall appraisal and evaluation for radiotherapy planning," Phys. Med. Biol. **26**, 81-99 (1981)..... 100, 101, 102

- R.E. Bentley , "Digital computers in radiation treatment planning," Br. J. Radiol. **37**, 748-755 (1964)..... 27, 28

- M. Boutillon and A. M. Perroche-Roux, "Re-evaluation of the W value for electrons in dry air," Phys. Med. Biol. **32**, 213-219 (1987).....12

- J. R. Cameron, N. Suntharalingam, and G. N. Kenney, *Thermoluminescent Dosimetry TLD*, (University of Wisconsin Press, Madison, WI, 1968).....59

- K. J. Cassell, P. A. Hobday, and R. P. Parker, "The implementation of a generalised Batho inhomogeneity correction for radiotherapy planning with direct use of CT numbers," Phys. Med. Biol. **26**, 825-833 (1981).....95

- C. Constantinou, J. C. Harrington, and L. A. DeWerd, "An electron density calibration phantom for CT based treatment planning computers," Med. Phys. 19, 325-327 (1992).....100, 103, 105

- D. W. Cope, R. E. Bentley, and J. Milan, "The use of a PDP-8 computer for on-line treatment planning," in *Computers in Radiology*, Proceedings of International Meeting in Brussels, 157-164 (1969).....6, 28

- J. R. Cunningham and J. Milan J, "Radiation treatment planning using a display-oriented small computer," in *Computers in Biomedical Research*, edited by R. W. Stacey and B. C. Waxman, vol 3, 159-179 (Academic Press, New York, 1969).....28

- H. Dahlin, I. L. Lamm, T. Landberg, S. Levernes, and N. Ulso, "User requirements on CT based computerized dose planning systems in radiotherapy," Acta. Radiol. Oncol. **22**, 398-415 (1983).....51

- R. G. Dale, "Implementation of the Philips treatment planning system for use in radiation therapy," Br. J. Radiol. **51**, 613-621 (1978).....7, 48, 49

- M. J. Day and G. A. Aird, "The equivalent-field method for dose determination in rectangular fields," Br. J. Radiol. Suppl. 17, 105-114 (1983).....40, 42

- R. E. Drzymala, "Quantitative analysis of treatment plans," in *3-D Radiation Treatment Planning and Conformal Therapy*, edited by J. A Purdy and B. Emami, 39-48 (Medical Physics, Madison, WI, 1993).....35

- M. D. C. Evans and L. J. Schreiner , "A simple technique for film dosimetry," Radiother. Oncol. **23**, 265-267 (1992).....59

- B. A. Fraass, D. L. McShan, and M. K. Martel, "Quality assurance for 3-D treatment planning," in *3-D Radiation Treatment Planning and Conformal Therapy*, edited by J. A. Purdy and B. Emami, 75-93 (Medical Physics, Madison, WI, 1993).....123, 125

- R. A. Geise and E. C. McCullough, "The use of CT scanners in megavoltage photon-beam therapy planning," Radiology **124**, 133 (1977).....105

- T. W. Holmes and E. C. McCullough, "Acceptance testing and quality assurance of automated scanning film desitometers used in the dosimetry of electron and photon therapy beams," Med. Phys. **10**, 698-700 (1983).....59

- W. F. Holmes, "External beam treatment planning with programmed console," Radiology **94**, 391-400 (1970).....28

- International Commission on Radiation Units and Measurements, ICRU Report No. 24. "Determination of absorbed dose in a patient irradiated by beams of x or gamma rays in radiotherapy procedures" (ICRU, Washington, D.C., 1976)..... 16, 19, 51, 97

- International Commission on Radiation Units and Measurements, ICRU Report No. 33. "Radiation quantities and units" (ICRU, Washington, D.C.,1980).....10, 11, 12, 102

- International Commission on Radiation Units and Measurements, ICRU Report No. 42. "Use of computers in external beam radiotherapy procedures with high-energy photons and electrons" (ICRU, Washington, D.C., 1987).....7, 30, 47, 51, 67, 71, 100

- International Commission on Radiation Units and Measurements, ICRU Report No. 44. "Tissue substitutes in radiation dosimetry and measurement" (ICRU, Washington, D.C., 1989)..... 102, 106

- International Commission on Radiation Units and Measurements, ICRU Report No. 48. "Phantoms and computational models in therapy, diagnosis and protection" (ICRU, Washington, D.C., 1992).....108

- International Commission on Radiation Units and Measurements, ICRU Report No. 50. "Prescribing, recording and reporting photon beam therapy" (ICRU, Washington, D.C., 1993).....5

- J. Jacky and C. P. White, "Testing a 3-D radiation therapy planning program," Int. J. Radiat. Oncol. Biol. Phys. **18**, 253-261 (1990).....7, 48, 123

- H. E. Johns and J. R. Cunningham, *The Physics of Radiology*, 4th ed. (Charles Thomas, Springfield, IL, 1983).....19, 30, 32, 88, 92, 102, 103, 104

- C. Kappas and J. C. Rosenwald, "Quality control of inhomogeneity correction algorithms used in treatment planning systems," Int. J. Radiat. Oncol. Biol. Phys. **32**, 847-858 (1995).....7, 48, 49, 99

- F. M. Khan, *The Physics of Radiotherapy*, 2nd ed. (Williams & Wilkins, Baltimore, MD, 1994).....88

- F. M. Khan, W. Sewchand, J. Lee, and J. F. Williamson, "Revision of tissue-maximum ratio and scatter-maximum ratio concepts for cobalt 60 and higher energy x-ray beams," Med. Phys. **7**, 230-237 (1980).....24

- A. Kosunen, H. Järvinen, S. Vatnitskij, I. Ermakov, A. Chervjakov, J. Kulmala, M. Pitkänen, T. Väyrynen, and A. Väänänen, "Intercomparison of radiotherapy treatment planning systems for external photon and electron beam dose calculations," Radiother. Oncol. **29**, 327-335 (1993).....7, 48, 49

- M. E. Masterson, G. Barest, C. Chen-Shou, K. Dopke, R. D. Epperson, W. B. Harms, K. E. Krippner, R. Mohan, E. D. Slessinger, M. R. Sontag, M. M. Urie, R. E. Wallace, and J. W. Wong, "Interinstitutional experience in verification of external photon dose calculations," Int. J. Radiat. Oncol. Biol. Phys. **21**, 37-58 (1991).....7, 48, 49, 117

- E. C. McCullough, "Photon attenuation in computed tomography," Med. Phys. **2**, 307-320 (1975).....101, 103

- E. C. McCullough, "Specifying and evaluating the performance of computed tomography (CT) scanners," Med. Phys. **7**, 291-296 (1980)..... 125

- E. C. McCullough and T. W. Holmes, "Acceptance testing computerized radiation therapy treatment planning systems: Direct utilization of CT scan data," Med. Phys. 12, 237-242 (1985)..... 100, 103

- E. C. McCullough and A. M. Krueger, "Performance evaluation of computerized treatment planning systems for radiotherapy external photon beams," Int. J. Radiat. Oncol. Biol. Phys. **6**, 1599-1605 (1980)..... 7, 48, 49, 51

- A. F. McKinlay, *Thermoluminescence Dosimetry*, Medical physics handbooks 5 (Adam Hilger Ltd., Bristol, UK, 1981)..... 60

- J. Milan and R. E. Bentley , "The storage and manipulation of radiation dose data in a small digital computer," Br. J. Radiol. **47**, 115-121 (1974)..... 28, 29, 36, 71

- H. C. Mota, C. H. Sibata, W. Roberts, and P. D. Higgins, "Film dosimetry: linearisation of dose-response for relative measurements of dose distribution," Phys. Med. Biol. **35**, 565-569 (1990)..... 62

- National Council on Radiation Protection and Measurements, NCRP Report No. 69. "Dosimetry of x-ray and gamma ray beams for radiation therapy in the energy range of 10 keV to 50 MeV" (NCRP, Bethesda, MD, 1981)..... 15

- R. P. Parker, P. A. Hobday, and K. J. Cassell, "The direct use of CT numbers in radiotherapy dosage calculations for inhomogeneous media," Phys. Med. Biol. **24**, 802-809 (1979)..... 100, 103

- Photon Treatment Planning Collaborative Working Group, "State-of-the-art of external photon beam radiation treatment planning," Int. J. Radiat. Oncol. Biol. Phys. **21**, 9-23 (1991)..... 33

- Photon Treatment Planning Collaborative Working Group, "Role of inhomogeneity corrections in three-dimensional photon treatment planning," Int. J. Radiat. Oncol. Biol. Phys. **21**, 59-69 (1991)..... 115

- C. Pla, E. B. Podgorsak, "A computerized TLD system," Med. Phys. **10**, 462-466 (1983)..... 60

- E. B. Podgorsak, M. Gosselin, M. Pla, T. H. Kim, and C. R. Freeman, "A simple isocentric technique for irradiation of the breast, chest wall and peripheral lymphatics," Br. J. Radiol. **57**, 57-63 (1984)..... 82

- E. B. Podgorsak, M. Pla, M. Gosselin, J. F. Guerra, and C. R. Freeman, "The McGill isocentric breast irradiation technique," Medical Dosimetry **12**, 3-7 (1987)..... 82

- S. C. Prasad, G. P. Glasgow, and J. A. Purdy, "Dosimetric evaluation of a computed tomography system," Radiology **130**, 777-781 (1979)..... 105

- *RFA 300 radiation field analyzer, operation manual* (Scanditronix AB, Uppsala, Sweden, 1992)..... 57, 59, 72

- *RK ionization chamber, reference documentation* (Scanditronix AB, Uppsala, Sweden, 1987)..... 57

- K. E. Sixel and E. B. Podgorsak, "Buildup region and depth of dose maximum of megavoltage x-ray beams," Med. Phys. **21**, 411-416 (1994)..... 14

- M. R. Sontag and J. R. Cunningham, "Corrections to absorbed dose calculations for tissue inhomogeneities," Med. Phys. **4**, 431-436 (1977)..... 94

- M. R. Sontag and J. R. Cunningham, "The equivalent tissue-air ratio method for making absorbed dose calculations in a heterogeneous medium," Radiology **129**, 787-794 (1978)..... 97, 98

- T. D. Sterling, H. Perry, and L. Katz, "Automation of radiation treatment planning-IV. Derivation of a mathematical expression for the percent depth dose surface of cobalt-60 beams and visualization of multiple field dose distributions," Br. J. Radiol. **37**, 544-550 (1964)..... 30, 40, 42

- P. Storchi and E. Woudstra, "Calculation models for determining the absorbed dose in water phantoms in off-axis planes of rectangular fields of open and wedged beams," Phys. Med. Biol. **40**, 511-527 (1995)..... 40, 43

- W. L. Tang, F. M. Khan, and B. J. Gerbi, "Validity of lung correction algorithms," Med. Phys. **13**, 683-686 (1986)..... 99

- J. Van Dyk, R. B. Barnett, J. E. Cygler, and P. C. Shragge, "Commissioning and quality assurance of treatment planning computers," Int. J. Radiat. Oncol. Biol. Phys. **26**, 261-273 (1993).....7, 47, 48, 49, 51, 52, 79, 124

- Varian Oncology Systems, *Installation and configuration guide document CADPLAN 2.62*, ver. 1.4 (Varian-Dosetek Oy, Espoo, Finland, 1995).....36

- Varian Oncology Systems, *External beam modeling reference manual CADPLAN 2.62*, ver. 1.1, (Varian-Dosetek Oy, Espoo, Finland, 1995).....40, 96

- S. Webb and R. A. Fox, "Verification by Monte Carlo methods of a power law tissue-air ratio algorithm for inhomogeneity corrections in photon beam dose calculations," Phys. Med. Biol. **25**, 225-240 (1980).....95, 99

- D. R. White, "An analysis of the Z-dependence of photon and electron interactions," Phys. Med. Biol. **22**, 219-228 (1977).....103

- D. R. White, R. J. Martin, and R. Darlison, "Epoxy resin based tissue substitutes," Br. J. Radiol. **50**, 814-821 (1977).....106

- J. F. Williamson, F. M. Khan, and S. C. Sharma, "Film dosimetry of megavoltage photon beams: A practical method of isodensity-to-isodose curve conversion," Med. Phys. **8**, 94-98 (1981)..... 66

- J. W. Wong and J. A. Purdy, "Review of methods of inhomogeneity corrections," in Advances in Radiation Oncology Physics: Dosimetry, Treatment Planning, and Brachytherapy, edited by J. A. Purdy, AAPM monograph 19, 886-899, (American Institute of Physics, New York, 1992).. 117

- M. E. Young and J. D. Gaylord, "Experimental tests of corrections for tissue inhomogeneities in radiotherapy," Br. J. Radiol. **43**, 349-355 (1970).....99